

Review

Versatile Nanoplatfoms with enhanced Photodynamic Therapy: Designs and Applications

Kai Yan^{1,2*}, Yabin Zhang^{3,4*}, Chenglong Mu¹, Qunna Xu¹, Xunan Jing², Daquan Wang², Dongfeng Dang², Lingjie Meng²✉ and Jianzhong Ma¹✉

1. College of Bioresources Chemical and Materials Engineering, Shaanxi University of Science and Technology, Xi'an 710021, China.
2. School of Science, Xi'an Key Laboratory of Sustainable Energy Material Chemistry, MOE Key Laboratory for Nonequilibrium Synthesis and Modulation of Condensed Materials, Xi'an Jiaotong University, Xi'an 710049, P. R. China.
3. Key Laboratory of Testing Technology for Manufacturing Process of Ministry of Education, Southwest University of Science and Technology, Mianyang 621010, P. R. China.
4. Institute of Textiles & Clothing, The Hong Kong Polytechnic University, Hung Hom, Kowloon, Hong Kong, China.

*These authors contributed equally to this work.

✉ Corresponding authors: E-mails: menglingjie@xjtu.edu.cn; majz@sust.edu.cn.

© The author(s). This is an open access article distributed under the terms of the Creative Commons Attribution License (<https://creativecommons.org/licenses/by/4.0/>). See <http://ivyspring.com/terms> for full terms and conditions.

Received: 2020.03.24; Accepted: 2020.05.20; Published: 2020.06.05

Abstract

As an emerging antitumor strategy, photodynamic therapy (PDT) has attracted intensive attention for the treatment of various malignant tumors owing to its noninvasive nature and high spatial selectivity in recent years. However, the therapeutic effect is unsatisfactory on some occasions due to the presence of some unfavorable factors including nonspecific accumulation of PS towards malignant tissues, the lack of endogenous oxygen in tumors, as well as the limited light penetration depth, further hampering practical application. To circumvent these limitations and improve real utilization efficiency, various enhanced strategies have been developed and explored during the past years. In this review, we give an overview of the state-of-the-art advances progress on versatile nanoplatfoms for enhanced PDT considering the enhancement from targeting or responsive, chemical and physical effect. Specifically, these effects mainly include organelle-targeting function, tumor microenvironment responsive release photosensitizers (PS), self-sufficient O₂ (affinity oxygen and generating oxygen), photocatalytic water splitting, X-rays light stimulate, surface plasmon resonance enhancement, and the improvement by resonance energy transfer. When utilizing these strategies to improve the therapeutic effect, the advantages and limitations are addressed. Finally, the challenges and prospective will be discussed and demonstrated for the future development of advanced PDT with enhanced efficacy.

Key words: photodynamic therapy, malignant tumor, versatile nanoplatfoms, microenvironment,

Introduction

Cancer is one of the greatest conundrums in the modern medical field, posing a great threat to human health [1-3]. Conventional cancer therapies include surgery [4], chemotherapy [5], and radiotherapy [6], which have pros and cons. Surgery fails to completely remove all tumor tissues, resulting in a high recurrence rate [7]. Chemotherapy usually lacks selectivity to cancer cells and typically causes multi-drug resistance [8]. Radiotherapy can damage healthy cells and tissues near cancer cells [9]. Thus, existing cancer treatment options have limited therapeutic

effects. Recently, new treatment modalities with improved efficacy and reduced adverse effects have received much attention, especially phototherapy dating back to three thousand years. The treatment of lupus vulgaris with a short-wavelength light by Niels Ryberg Finsen was awarded the Nobel Prize in 1903, instigating the development of phototherapy [10], which is a minimally invasive, controllable technique that relies on the phototherapeutic agents in conjunction with light irradiation to kill cancer cells selectively [11-13]. As two typical phototherapy

approaches, photodynamic therapy (PDT) and photothermal therapy (PTT) have been extensively studied and are commonly used. PTT agents absorb a selective wavelength of light and dissipate the absorbed energy through non-radiative decay that increases the temperature in the local environment, leading to the thermal ablation of cancer cells [14, 15]. However, in the actual treatment process, excessive heat tends to damage normal cells and tissues, causing complications and negatively affecting the treatment.

Despite its shortcomings, PDT has become a promising therapeutic option by using photosensitizers (PS) and light irradiation to induce cell death and tissue destruction [16]. Upon exposure to appropriate wavelength light, the PS can transfer energy to surrounding oxygen molecules and produce cytotoxic reactive oxygen species (ROS), such as singlet oxygen ($^1\text{O}_2$), superoxide, hydrogen peroxide (H_2O_2), and hydroxyl radicals, which efficiently eliminate highly proliferating cells by severe and irreversible damage to their organelle [17, 18]. PDT has been extensively studied in the treatment of both premalignant and malignant skin tumors [19, 20], head [21] and neck [22, 23], prostate [24, 25], non-small-cell lung [26, 27], and other cancers. Due to the high cytotoxicity of the generated $^1\text{O}_2$, PDT can generate much greater treatment effects than PTT. Compared to the widely used chemotherapy and radiotherapy, PDT entails beneficial features like reduced side effects on normal tissues, possible repeatable doses, and absence of scarring [28, 29]. Considering these merits, PDT has been under the research spotlight for in-depth investigation as an important paradigm for a variety of cancers and non-cancerous lesions in recent years.

Despite considerable progress in its use for cancer treatment, a few outstanding issues for the efficacy of PDT include PS utilization efficiency, light penetration depth, and endogenous oxygen generation in tumors [30-32]. The hypoxia in tumor tissues, caused by the abnormal vasculature perfusion, uncontrollable cell proliferation, and dysfunctional lymphatic system, significantly impairs the PDT outcome [33, 34]. Conversely, PDT aggravates the hypoxia in the tumor microenvironment because of oxygen depletion and the vascular shutdown effect, finally triggering tumor metastasis and tumor recurrence [35, 36]. Besides, the antioxidative glutathione (GSH) overexpressed in cancer cells can scavenge the generated ROS, thus lowering PDT efficacy. To address these issues and deliver the PS molecules to the desired site, several new approaches have been considered for maximizing the efficacy of PDT. The integration of

nanotechnology with material science has led to the extensive application of nanoplateforms in medicine [37-39], especially nanoplateform-based drug delivery systems. These systems show diagnostic and therapeutic prospects in clinical applications due to the localization ability, high-efficiency, low-toxicity, and controlled release of drugs [40, 41]. More specifically, PDT, combined with nanosystems has become a hot spot in the prevention, diagnosis, treatment, and monitoring of tumors. Such nanoplateforms are elaborately constructed to achieve enhanced PDT for specific targeting, high drug loading, and multi-functional integration [42-44].

This review aims to provide an overview of nanotherapeutic advancements for enhanced PDT targeted towards tumor therapy in the last five years (Figure 1). We categorize functional polymer nanoplateforms to achieve specific accumulation of PS in tumors to enhance PDT, such as targeting performance, responsive release, and charge turnover. High-efficiency PDT of self-oxygenation systems (carrying oxygen and generating oxygen) and photocatalytic hybrid nanoplateforms are summarized. Also, enhanced PDT with nanoplateforms using X-rays, plasmon resonance and other physical methods have been outlined. Finally, we highlight the challenges and possible developments of nanoplateforms for enhanced PDT, which could inspire the design of nanoplateforms and prompt clinical applications of PDT in tumor therapy.

Targeted and responsive nanoplateforms for enhanced PDT

Targeting nanoplateforms

When the nanoplateforms are injected into the biological tissue, they are often recognized as intruders by the immune system, provoking an immune response [45]. Also, the nanoplateforms are likely to be picked up and cleared out by the mononuclear phagocyte system during blood circulation, leading to shortened circulation time and limited therapeutic effects [46]. The nontargeting nanoplateforms can passively target the tumor through enhanced permeability and retention (EPR) effect and, therefore, can deliver a small amount of nanomedicine to the tumor sites. On the other hand, nanoplateforms endowed with targeting ability can achieve specific and improved delivery to tumor tissues. Another important aspect of PDT is that the PS is taken up by different subcellular organelles such as the mitochondria, lysosomes, endoplasmic reticulum, Golgi apparatus, and plasma membranes [47, 48] and under light irradiation, its subcellular localization largely determines the damage produced

by ROS. Thus, it would be of great interest to exploit targeted nanoplateform delivery systems to transport PS directly into the desired subcellular organelles [49].

Cell membrane is the most important protective barrier in living cells maintaining cell integrity and guarantees the essential cellular functions [50, 51]. Severe damage to the plasma membrane induces cellular apoptosis, necrosis, and autophagy. Cell membrane-targeted therapy can be more efficient because it does not require endocytosis of drugs. Moreover, many shortcomings of conventional chemotherapy, such as the intracellular degradation of drugs or drug resistance-induced failures, can be avoided [52]. A novel charge reversible self-delivery chimeric peptide C₁₆-PRP-DMA (C₁₆-K(PpIX)RRK (DMA)K(DMA)-PEG-COOH) was designed for long-term cell membrane-targeted PDT (Figure 2A). The self-assembled nanoparticles could stay on the cancer cell membrane for a long time because of the synergetic effect of alkyl chain palmitic acid and positively charged RRKK attached to the cell membrane [53]. Under light irradiation, the ROS generated by the inserted C₁₆-PRP-DMA directly disrupted the cell membrane and rapidly caused cell necrosis, remarkably increasing the PDT effect *in vitro* and *in vivo*. To maximize the therapeutic potency, a self-transformable pH-driven, membrane-anchoring nanoplateform was constructed by attaching protoporphyrin IX (PpIX) to the end of the water-soluble peptide [54]. Benefiting from the insertion peptide, the nanoplateform could form an α -helix structure under acidic conditions (pH 6.5 or 5.5), but remained random coil at normal pH of 7.4. This feature enabled successful insertion of nanoplateforms into the membrane lipid bilayer, especially for cancerous cell membranes in the acidic tumor microenvironment. Under laser irradiation at 630 nm, the plasma membrane was severely damaged by *in situ* generated ROS, subsequently inducing cell death [54]. In particular, *in vivo* studies indicated the high inhibition effect of this nanoplateform against primary tumors and the successful prevention of tumor metastasis.

Nucleus is the most significant organelle in the cell and contains most of the intracellular genetic materials [55]. Any disruptions inside the nucleus would subsequently affect the cellular DNA disturbing the highly regulated cell cycle. Consequently, nuclear-targeted strategies could facilitate the penetration of the PS into the nucleus and greatly improve therapeutic efficiency. As shown in Figure 2B, Shi's group *et al.* made TAT and RGD peptides co-conjugated with mesoporous silica nanoparticles (MSNs) as PDT carriers [56]. TAT peptides enabled the nuclear penetration of

mesoporous silica nanoparticles for efficient accumulation of the PS inside the nuclei. Upon irradiation, the intranuclearly accumulated PS could generate ROS to destroy DNA instantaneously. Moreover, the co-conjugated RGD peptides endowed the nuclear-targeted delivery system with recognition of and specific binding to tumor vasculature and tumor cell membranes for significantly enhanced specificity and reduced side effects. As is evident from Figures 2B2 and 2B3, the nuclear-targeted nanoplateforms exerted substantially stronger inhibition effect on tumor growth than Ce6@MSNs-RGD, Ce6@MSNs, and free Ce6. Taking advantage of structural programmability and biocompatibility, self-assembled DNA nanostructures have attracted much attention in biomedical applications. Yang *et al.* developed nanoscale coordination polymers (NCPs) based on the interaction between calcium ions (Ca²⁺) and AS1411 DNA G quadruplexes [57]. Both Ce6 and an iron-containing porphyrin inserted into the G-quadruplex structure. The NCPs enabled the intranuclear transport of Ce6 to generate ROS inside cell nuclei. AS1411 inhibited the expression of antiapoptotic protein B-cell lymphoma 2 (Bcl-2), allowing for greatly improved PDT-induced cell apoptosis. Furthermore, the catalase-mimicking DNA enzyme function of G-quadruplexes and hemin could react with tumor endogenous H₂O₂ to generate oxygen for enhanced PDT by overcoming the hypoxia-associated resistance.

Mitochondria is the primary source of cellular ROS production (approximately up to 90%), which plays vital roles in energy production and cell apoptosis [58, 59]. Moreover, mitochondria could be susceptible to excessive ROS. The initial formation of ROS-induced changes in mitochondrial permeability, depolarization, deformation, and release of cytochrome C, ultimately resulted in apoptosis [60, 61]. Therefore, a PS delivery system targeting mitochondria is greatly beneficial for enhancing the photodynamic therapeutic effect. The peptide Ad-CGKRRK-GFLG-EE-HAIYPRH(T7) with a guest molecule Ad termination and cathepsin B (CTSB) (overexpressed in cancer cells)-cleavable linker GFLG was developed, and Ce6 was conjugated to the host molecule β -Cyclodextrin (β -CD) through an amide bond. Through CD/Ad recognition, CD-Ce6 and Ad-CGKRRK-GFLG-EE-HAIYPRH (T7) inclusion complexation self-assembled into supramolecular nanoplateforms [62]. T7 modification endowed supramolecular nanoplateforms with targeting ability for MCF-7 cancer cells. After internalization, the cleavage of the GFLG sequence by overexpressed CTSB exposed the mitochondria-targeting peptide CGKRRK allowing the accumulation of nanocarriers in

mitochondria and enhancing the PDT effect. Another mitochondria and plasma membrane dual-targeting nanoplatfrom was developed using the chimeric peptide for single-agent synergistic PDT [63], which included a hydrophobic photosensitizer PpIX, a bioactive peptide sequence with dual targeting function, and a hydrophilic poly (ethylene glycol) (PEG) chain. This amphipathic chimeric peptide could form spherical micelles by self-assembly in aqueous solution, with high drug loading efficacy as well as the excellent ability to produce ROS. Plasma membrane-targeting PDT increased the membrane permeability to improve the cellular delivery of nanoplatforms, and even directly disrupted the cell membrane to induce cell necrosis. Additionally, mitochondria-targeted PDT reduced mitochondrial membrane potential and significantly promoted cell apoptosis. Consequently, the dual-targeting property facilitated the effective subcellular localization of PpIX to generate ROS for enhanced PDT.

Lysosomes are important subcellular acidic organelles for cellular homeostasis, whose dysfunction is responsible for several diseases [64]. There is ample evidence to verify that the lysosomal death pathway could contribute to the programmed cell death sensitivity of cancer cells [65]. Xiang *et al.* developed novel cancer cell lysosome-targetable NO-delivery nanoplatforms composed of a ruthenium nitrosyl donor (Lyso-Ru-NO), a cancer cell directing

group of folic acid, and a carrier of biocompatible carbon-doped titanium dioxide nanoparticles (Figure 2C) [66]. The ruthenium nitrosyl Lyso-Ru-NO group contained the Lyso-NINO ligand, wherein a morpholine moiety targeted the lysosomes. The incorporation of folic acid and morpholine groups rendered it capable of targeting folate-receptor overexpressing-cancer cells and specifically accumulating in the subcellular lysosomal organelles, where 808 nm NIR light irradiation simultaneously released NO and ROS. The cytotoxicity assay showed that the dual-targeted nanoplatforms have the highest anticancer efficacy compared to their nontargeted counterparts under NIR light sensitization. To further compare differences in mitochondria- and lysosome-targeted PDT, two PS were designed based on iridium (III) complex (Ir-P(ph)₃ and Ir-alkyl group, which specifically targeted the mitochondria and lysosomes, respectively. The results indicated that HeLa cells treated with the mitochondria-targeted complex kept a slower respiration rate, resulting in a higher intracellular oxygen level under hypoxia. Consequently, this complex showed an enhanced PDT effect compared to the lysosome-targeted complex, especially under hypoxic conditions [67]. It is possible that the mitochondria-targeted PS inhibited mitochondrial respiration, leading to higher intramitochondrial oxygen content, and, therefore, is more beneficial for PDT in hypoxic tumor cells.

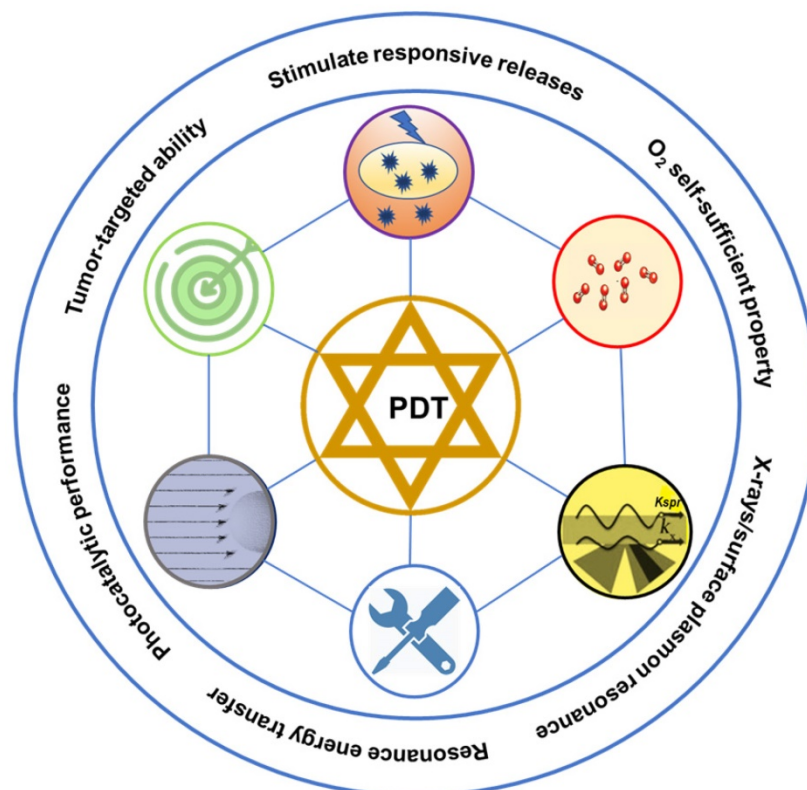


Figure 1. Schematic illustration of the versatile nanoplatforms for enhanced PDT.

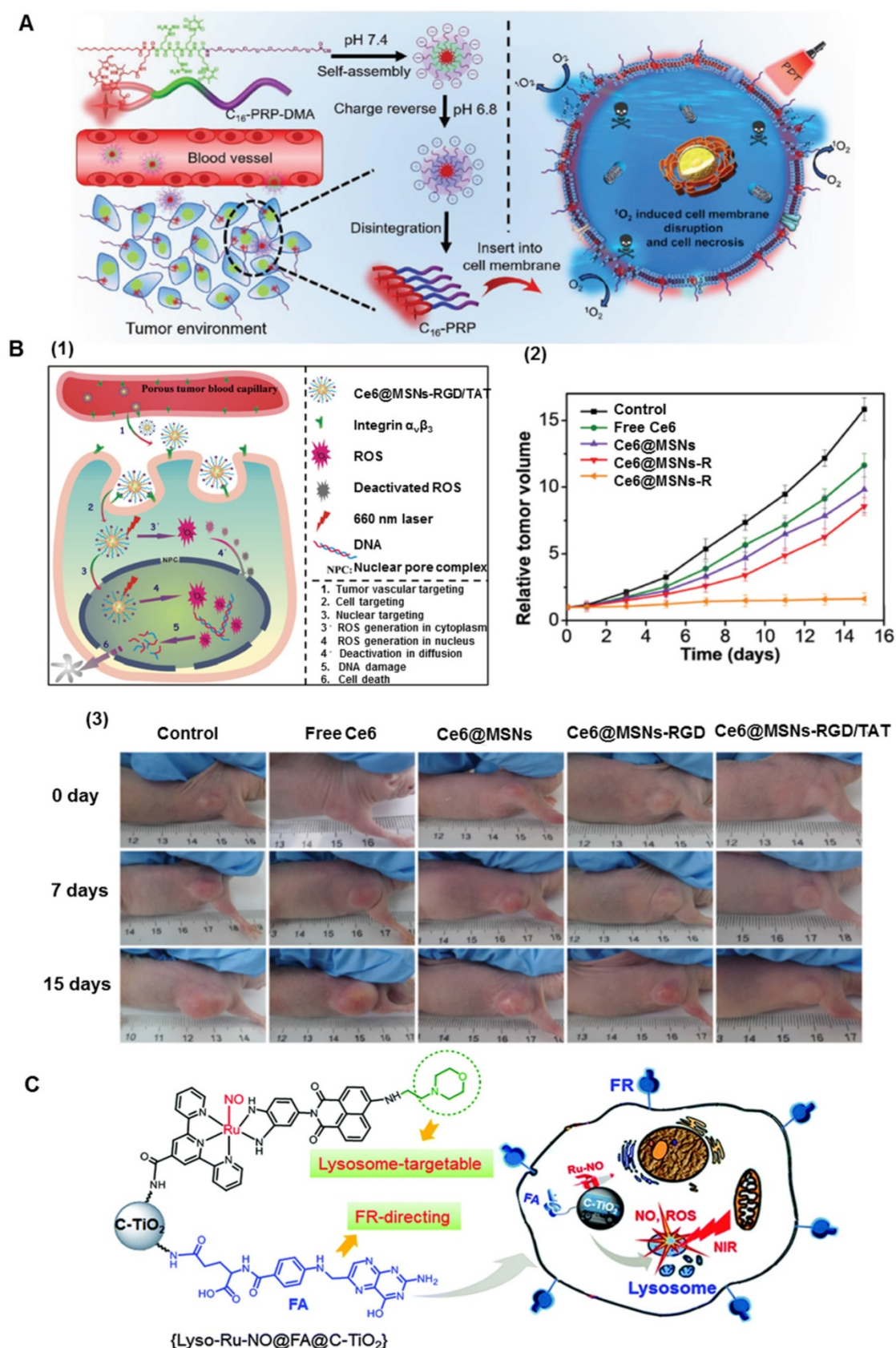


Figure 2. A. Membrane-anchoring PS for enhanced PDT. Self-assembly of chimeric peptides into nanoparticles and the charge reverse at tumor environment (left), resulting in cell membrane disruption and cell necrosis (right). Adapted with permission from ref. [53]. Copyright 2017 Wiley-VCH. B. Intracellular PS delivery and PS for enhanced PDT. (1) Schematic illustration of sequential-targeted PDT based on $Ce6@MSNs-RGD/TAT$. (2) Tumor growth curves of different groups of tumor-bearing mice after PDT. (3) Photographs of the mice taken after 0 day, 7 and 15 days of PDT. Adapted with permission from ref. [56]. Copyright 2014 Wiley-VCH. C. Schematic representation of nanoplatforms and the directed attack of cancer cell lysosomes by NO and ROS under near infrared (NIR) light irradiation. Adapted with permission from ref. [66]. Copyright 2016 Royal Society of Chemistry.

Apart from organelle-targeting nanoplateforms, other nanoplateforms can also achieve enhanced PDT. Macrophages are highly abundant in the stroma of solid tumors and have been demonstrated to play an important role in the development and progression of cancer [68]. Moreover, macrophages can enrich much more PS than tumor cells, making the PDT effect greatly potentiated when the tumors are treated with PS with a macrophage-activating factor. C-Phycocyanin, a macrophage-targeting agent, has been widely used in food, cosmetics, and biomedical applications due to its good biocompatibility, non-toxicity, water-solubility, unique color, strong absorption in the visible region (550-650 nm), and high fluorescence quantum yield. When combined with unsubstituted zinc phthalocyanine, it could facilitate PS for PDT. Furthermore, this conjugation exhibited an enhanced photodynamic effect due to the improved solubility and aggregation of zinc phthalocyanine [69]. Thus, C-Phycocyanin can act as both a new class of tumor-associated macrophages PS and a desirable nanoplateform for other therapeutic agents. Besides, lactoferrin is a member of the transferrin family and commonly found in blood plasma, and has a potential role in treating diseases because of its antioxidant, antitumor, antiviral, and antifungal properties. Adimoolam *et al.* loaded Ce6 into lactoferrin by the water-in-oil emulsion method [70]. The yield of reactive oxygen was enhanced in the nanoplateforms compared to free Ce6. Also, specific Ce6 release at low pH and higher uptake and intracellular concentrations of Ce6 compared with free Ce6 *in vitro* were observed. Upon exposure to light, the nanoplateforms caused light-mediated cell death in the SK-OV-3 and MDA-MD 231 cells.

Compared to free Ce6, it showed a substantial decrease (44 times) in the Ce6 requirement.

Despite significant advancements, targeted therapeutic agents are still limited to clinical applications. The development of malignant tumors is an extremely complicated process. It involves multiple genes and new gene mutations evolve in a multistep process, increasing the difficulty of targeted therapy. Targeted tumor agents show considerable toxicity to the digestive tract and vasculature with a negative impact on the therapeutic effect. To overcome the defects in targeted therapy, the joint application of various targeted drugs might show a better outcome.

Responsive nanoplateforms for enhanced PDT

Efficient cellular internalization of the nanoplateforms and on-demand release of the PS are two significant steps for efficacy enhancement [71, 72]. A high degree of cellular uptake can guarantee the maximal amount of intracellular PS, whereas rapid cargo release can address the problem from the limited diffusion distance as well as the short half-life of $^1\text{O}_2$. It is vital to design responsive nanoplateforms to enhance cellular uptake and control PS release. So far, exogenous (externally applied) stimuli to trigger PS release, such as temperature [73, 74], light [75, 76], and magnetic triggers [77, 78], have been explored widely. Besides, tumor pathophysiology displays characteristic changes such as pH [79], enzyme activity [80], or redox properties [81], and allowing opportunities to exploit these endogenous factors as internal stimuli. Table 1 summarizes targeted and responsive nanoplateforms for enhanced PDT.

Table 1. Targeting and responsive nanoplateforms for enhanced PDT

Nanoplateforms design	PS	Enhanced mechanism	Improved therapeutics	Ref
Chimeric peptide	Ce6	Cell membrane target	PDT	53
Peptide	PpIX	pH-driven membrane-anchoring	PDT	54
SiO ₂ -TAT/RGD	Ce6	Nuclear-targeted delivery	PDT	56
Coordination polymers	Ce6	Nuclear-targeted drug delivery	PDT	57
Supramolecular nanocarriers	Ce6	Mitochondria-target	PDT	62
Chimeric peptide	PpIX	Mitochondria/plasma membrane-target	PDT	63
Lyso-Ru-NO@FA@C-TiO ₂	C-TiO ₂	Lysosome-targeted delivery	PDT	66
Iridium(III) complexes	Ir-P(ph) ₃ /Ir-alkyl	Mitochondria /lysosome target	PDT	67
C-Phycocyanin-ZnPc conjugates	ZnPc	Macrophage-target	PDT	69
Pseudopolyrotaxane micelles	PpIX	pH-responsive release	PDT	88
Polymeric micelles	Ce6	pH-responsive/EGFR targeting peptides	PDT	89
Coordination polymer nanoparticles	ZnPc	Charge-reversal	PDT	92
Supramolecular amphiphiles	Ce6	Redox-responsive	PDT	101
Amphiphilic polymers	Ce6	Redox stimulation	PDT	102
Nano-MOF with Cu ^{II}	Porphyrin	Reducing of GSH	PDT	105
BSA-MBPB	Methylene blue	H ₂ O ₂ -activatability	PDT	106
HA-Ce6 conjugation	Ce6	Hyaluronidase	PDT	109
Polymer vesicles	Nile blue	Enzyme simulation	PDT	111
Amphiphilic block copolymer	Ce6	Singlet oxygen-sensitive	Chemo-PDT	117
Polymeric micelles	Ce6	Hypoxia/Singlet oxygen responsive	PDT	118
Dopamine-reduced graphene oxide	Ce6	Photothermal responsive	PDT/PTT	133

Tumor microenvironment (pH and GSH)-responsive nanoplatforms

The microenvironment of cancerous tissues is specific and markedly different from that of the extracellular matrix and normal tissues. pH is one of the stimuli that has been most frequently utilized to control intracellular drug delivery in specific organs based on environmental changes induced by pathological conditions [82, 83]. Furthermore, the pH difference can be found in some organelles, such as endosomes (pH lower than 4.5) and lysosomes (~pH 5.5), where it is much lower than other intracellular organelles [84, 85]. Due to the pH gradient between the tumor microenvironment (pH \approx 6.5) and the physiological environment (pH \approx 7.4), the pH-responsive nanoplatforms undergo conformational changes through various mechanisms, such as protonation [86], charge reversal, or cleavage of a chemical bond [87], facilitating tumor-specific cell uptake or drug release. Such responsive nanoplatforms are usually fabricated through physically encapsulating or chemically conjugating the PS. So far, a variety of pH-responsive nanoplatforms have been designed to exploit low extracellular pH_{ex} or endosomal pH_{en} . For example, Tong *et al* attached 5-aminolevulinic acid (ALA) to α -cyclodextrin (α -CD) through an acid-labile hydrazone bond. Subsequently, the pH-responsive, cell-penetrating peptide R6H4 (RRRRRRHHHH) was conjugated to PEG to form PEG-R6H4. As shown in Figure 3A, dual pH-responsive ALA pseudo-polyrotaxane prodrug micelles were developed by the host-guest interaction of α -CD and PEG. Taking advantage of the pH-responsive R6H4, the nanoplatforms were easily internalized into tumor cells. Furthermore, ALA was released by the cleavage of the hydrazone bond at endo/lysosomal pH and further converted to PpIX for enhanced PDT [88]. To achieve multifunctionality, Chu *et al* used pH-responsive copolymers poly(ethylene glycol) methacrylate-co-2-(diisopropylamino)ethyl methacrylate, biodegradable copolymers methoxypoly(ethyleneglycol)/poly(ϵ -caprolactone), and maleimide-modified biodegradable copolymers to prepare new micelles. After entrapping the photosensitizer Ce6, the micelles were coated with the epidermal growth factor receptor (EGFR)-targeting peptide GE11, and showed enhanced PDT efficacy [89]. This could be attributed to the increased Ce6 uptake due to GE11 targeting and increased release of Ce6 for improved elimination of cancer cells in the acidic tumor microenvironment.

Recently, pH-dependent charge reversal delivery nanoplatforms exhibited great superiority in controlled release and targeted drug delivery [90].

The surface charge of nanoplatforms plays a decisive role in cell internalization and blood stability. The nanoplatforms can keep their original negatively charged status under neutral conditions in the bloodstream, thus preventing nonspecific interactions with serum proteins and normal tissues [91]. Upon arriving at the tumor tissues or endo/lysosomes, the original negative charge can quickly convert into positively charged status, thus triggering the efficient cell internalization. For example, tumor pH-sensitive photodynamic nanoplatforms $NaYF_4:Yb,Er@CaF_2$ were comprised of self-assembled, PS-grafted, pH-responsive polymeric ligands [92], which were prepared by derivatizing poly(ethylene glycol)-poly(β -benzyl-L-aspartate) with 1-(3-aminopropyl)imidazole, 3-phenyl-1-propylamine, and Ce6. The nanoplatforms were negatively charged without any discernible photoactivity at normal blood pH of \approx 7.4 but quickly switched their surface charge from negative to positive at an extracellular tumor pH of \approx 6.5. These nanoparticles not only exhibited enhanced tumor-cell internalization due to charge reversal but disassembled into well-dispersed nanoparticles in the endo/lysosomes of tumor cells, thus enabling efficient PDT. Besides, charge-reversal phthalocyanine-based coordination polymer nanoplatforms (PCPNs@Lip/DLC) were developed to improve the curative effect of PDT [93]. Tetra(4-carboxyphenoxy)-phthalocyaninatozinc coordinated with zinc was coated with a self-assembled lipid bilayer (Figure 3B), and 1,2-dicarboxylic-cyclohexane anhydride-modified lysyl-cholesterol (DLC) was functionalized on the surface of PCPN, endowing it with a charge-reversal ability. When exposed to a mildly acidic environment in the tumor tissue, DLC could degrade and enabled increased tumor uptake of PCPN due to the electrostatic interaction with the negatively charged cell membrane. The nanoplatforms were verified to enhance tumor cellular uptake and generate increased intracellular ROS after irradiation. As confirmed by *in vitro* and *in vivo* studies, the nanoplatforms remarkably increased the PDT effect. Despite the obvious potential of pH-sensitive nanoplatforms, they sometimes need to be combined with other stimuli to achieve precise and specific drug release at the targeted tumor sites.

Besides the difference in pH environment, the intracellular glutathione (GSH) level of cancer cells has been widely reported to be considerably higher (about 10 mM) than that in the extracellular matrix (about 2 μ M) [94, 95]. GSH can be used as a reducing agent due to the thiol groups and is an important antioxidant that can prevent the damage to the cellular components induced by ROS [96]. Previous reports have indicated that high intracellular GSH

levels in tumor cells can effectively trigger drug release [97, 98], facilitating efficient PS uptake from the functional nanoplateforms. Disulfide, selenium, or tellurium-containing nanoplateforms were exploited as redox-responsive drug-delivery systems [99, 100]. Zhang *et al.* developed supramolecular host-guest complexation between a PEG-functionalized pillararene and a pyridinium-terminated porphyrin derivative-bearing disulfide bond [5]. The supramolecules could self-assemble into spherical micelles with good colloidal stability, which exhibited the rapid release of porphyrin PS in a reducing environment. *In vitro* cytotoxicity confirmed that the supramolecular amphiphiles exhibited superior cellular uptake and remarkably enhanced PDT [101]. Another biocompatible stimuli-activated photosensitive nanoplateform (PEG-TPP-DNB) based on porphyrin molecules was designed (Figure 4A1). 5, 15-bis(4-aminophenyl)-10,20-diphenylporphyrin was regarded as the center of molecular structure and further modified at both ends with PEG chain and the functional group 2,4-dinitrobenzene via pH-deionized and thiol-labile sulfonamide linkages. Because nitrobenzene has a strong ability to withdraw electrons on the porphyrin macrocycles, the nanoplateforms remarkably quenched the fluorescence and $^1\text{O}_2$. Therefore, the redox-sensitive and activated nanoplateforms could minimize the biological imaging background and phototoxicity to normal tissues. In aqueous media, the amphiphilic nanoplateforms could self-assemble into nanomicelles and dissociate in response to the reductive thiol such as GSH. *In vivo* bioimaging further elucidated that the micelles showed selective tumor imaging and targeted PDT antitumor effect as well as low systemic toxicity (Figure 4A2). Overall, the amphiphilic nanoplateforms not only afforded targeted release of PS for maximized tumor enrichment but also exhibited excellent tumor-targeting PDT efficacy [102].

Although GSH stimulates the responsive nanoplateforms to release PS for enhanced PDT, the high concentration of GSH decreases ROS generation in cells, reducing the effectiveness of PDT. It has been demonstrated that a decrease in GSH concentration in tumor tissues could promote the ROS level by using nanoplateforms [103, 104]. A nano-metal-organic framework (MOF) was designed to enhance PDT. Cu^{II} as the active center of MOF could specifically bind and absorb GSH, thus directly reducing the intracellular GSH concentration and increasing the ROS level. Simultaneously, the porphyrin ligand could be used as the PS to generate abundant ROS under light irradiation. *In vitro* experiments indicated that MOF was readily taken up by breast cancer cells, and high ROS levels were produced under light

irradiation. This synergistically-increased ROS concentration accelerated apoptosis, enhancing the effect of PDT [105]. Using a similar enhancement mechanism, Zeng *et al.* incorporated a p-phenylboronic ester (PB) into the clinical PS methylene blue with a carbonochloridate PB-Cl, and encapsulated them within BSA to achieve imaging-guided tumor-targeted effective PDT (Figure 4B1). In the presence of H_2O_2 , the resultant caged nanoplateforms underwent H_2O_2 -mediated boronic ester oxidation, releasing the hydrophilic methylene blue to produce $^1\text{O}_2$, and quinoned methide rapidly deactivated GSH boosting the $^1\text{O}_2$ yield, thus synergistically strengthening the efficacy of PDT. Furthermore, the BSA-MBPB nanoplateforms could also recover the fluorescent and photoacoustic dual-modal imaging of the tumor region and precisely guide the tumor-selective PDT [106] (Figure 4B2 and 4B3).

Enzyme-responsive nanoplateforms

Enzyme-responsive nanoplateforms have been increasingly utilized for PDT because they could selectively and efficiently involve in all physiological, metabolic, and pathological processes [107]. Several studies have shown that hyaluronidase (HAase) enables the degradation of extracellular matrix to enhance therapies by increasing intratumor penetration of the drugs, and modulates the hypoxic tumor microenvironment [108]. A smart hyaluronidase-activated theranostic nanoplateform was prepared based on hyaluronic acid (HA) coupled with Ce6 using adipic dihydrazide (ADH). This nanoplateform could be specifically degraded and released by hyaluronidase in the tumor, exhibiting higher fluorescence and photoacoustic intensity than free Ce6. Additionally, this HA-based nanoplateform showed more effective PDT than free Ce6 to suppress tumor growth *in vitro* and *in vivo* [109]. Besides, the NQO1-based nanoplateforms also generated increasing attention as NQO1 is upregulated (~2-50-fold) in breast, pancreatic, colorectal, cervical, and lung cancers [110]. Yao and co-workers developed self-assembled vesicles from amphiphilic block copolymers containing quinone trimethyl lock-capped self-immolative side linkages and quinone-bridged Nile blue in the hydrophobic block [111]. Initially, their fluorescence emission and PDT potency were in the "off" state due to dye aggregation-caused quenching and quinone-rendered photoinduced electron transfer quenching. After internalization into NQO1-positive vesicles, the cytosolic NQO1 enzyme triggered the cleavage of quinone linkages and fluorogenic release of conjugated PS, resulting in NIR fluorescence emission turn-on and enhanced PDT.

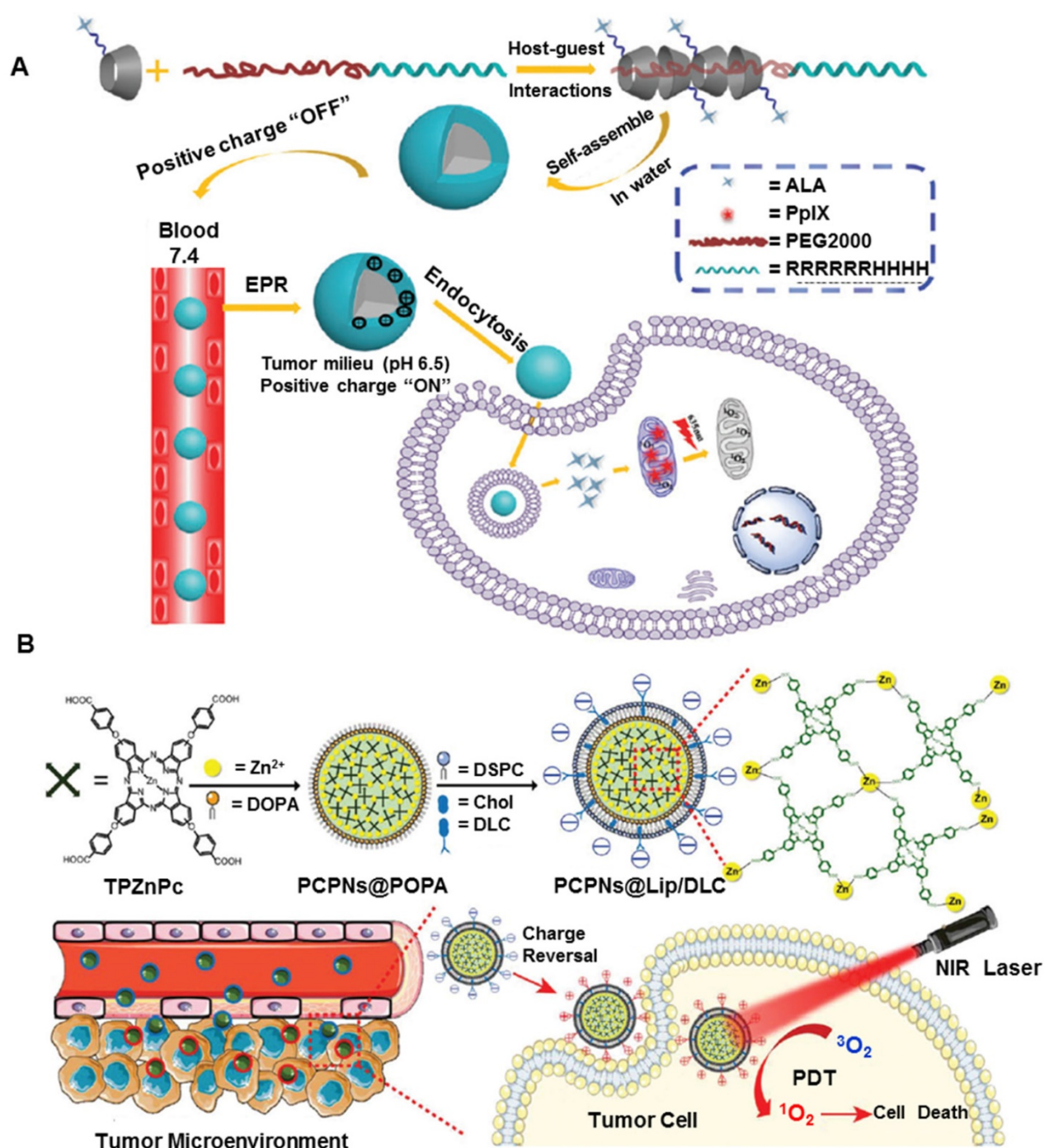


Figure 3. A. Schematic illustrations of ALA pseudopolyrotaxane prodrug micelles. Adapted with permission from ref. [88]. Copyright 2016 Royal Society of Chemistry. B. Schematic illustrations of PCPNs@Lip/DLC for enhanced PDT. Adapted with permission from ref. [93]. Copyright 2017 Royal Society of Chemistry.

ROS-responsive nanoplatforms

ROS plays a vital role in the physiological and pathophysiological processes of the human body [112]. It is also essential for the growth, development, and adaptation of organisms. In normal conditions, low concentrations of ROS regulate cell-signaling pathways and promote cell proliferation, whereas high levels of ROS induce oxidative stress that can disrupt the steady-state of cells and damage cellular

components including membrane lipids, proteins, DNA, and other biological molecules [113, 114]. Therefore, a lack of ROS or an excess of ROS may induce several abnormalities, including autoimmune, cardiovascular, and neurodegenerative diseases [115, 116]. This abnormal biochemical alteration in the disease sites has inspired studies on unbalanced ROS levels for developing target-specific drug delivery systems. By utilizing ROS-responsive materials and linkers, various ROS-responsive drug delivery

systems have been developed for therapeutic purposes. $^1\text{O}_2$ -responsive nanoplatforms are particularly appealing because of the highly reactive nature of $^1\text{O}_2$ and the rapid onset of responsive cascade events. Guruswamy *et al.* designed a novel biocompatible visible-light-responsive amphiphilic poly(ethylene glycol)-block-poly(caprolactone) copolymer by incorporating an $^1\text{O}_2$ -sensitive vinyl dithioether linker between the hydrophilic segments and the hydrophobic block [117]. The amphiphilic micelles could disassemble the nanostructure due to $^1\text{O}_2$ generated by visible light, and further release Ce6 and anticancer drug doxorubicin (DOX) for enhanced PDT. To further regulate the release of PS for improved PDT, Li *et al.* developed a methoxy poly(ethylene glycol)-azobenzene-poly(aspartic acid) copolymer conjugated with imidazole as the side chains [118]. The azobenzene and imidazole are hypoxia- and singlet oxygen-responsive (SR) moieties, respectively. The facilitated cellular uptake of micelles was realized by triggering azobenzene collapse that provoked PEG shedding, while Ce6 could be released rapidly by micelle disassembly from imidazole oxidation (Figure 5A). The $^1\text{O}_2$ -mediated cargo release not only overcame the limited diffusion range and short half-life of $^1\text{O}_2$ but also decreased the oxygen level, which could, in turn, enhance internalization and increase the intracellular Ce6 concentration. *In vivo* imaging study demonstrated that more Ce6 were accumulated in the tumor from dually responsive (DR) micelles in contrast to free Ce6 (Figure 5B). *In vivo* efficacy study indicated that the multifunctional micelles could maximize the PDT antitumor efficacy via interactively triggered delivery of the PS (Figure 5C).

Photothermal-responsive nanoplatforms

A photothermal responsive system induced by NIR light has gained acceptance for drug delivery in consideration of high efficiency, the noninvasive modality to tumor treatment, as well as the high spatial resolution of NIR light [119, 120]. Photothermal-response nanoplatforms also contribute to diffusion therapy of PS. Importantly, this system exhibits synergistic cancer therapy associated with hyperthermia and heat-induced local drug release. Recent photothermal nanoplatforms mainly include noble metallic nanoparticles (gold nanocages [121], gold nanorods [122]), semiconductor nanocrystals (CuS [123], WS_2 [124], and MoS_2 [125]) as well as carbon-based nanoparticles (carbon nanotubes [126], graphene [127], and carbon nanospheres [128]), organic dye molecules (ICG [129], IR780 [130]), and organic semiconducting polymer nanoparticles (polypyrrole [131], PEDOT:PSS [132]). Fu *et al.*

developed a novel tumor-targeting photothermal heat-responsive nanoplatform by using dopamine-reduced graphene oxide nanosheets (rGO-PDA), mesoporous silica-coated on the rGO-PDA surface to load Ce6, and hyaluronic acid as a gate-keeper as well as a targeting moiety [133]. The nanoplatforms showed excellent photothermal conversion ability under near-infrared radiation and controllable Ce6 release with an NIR irradiation response. It could specifically deliver Ce6 to CD-44 over-expressing cancer cells for PDT. The combination of excellent NIR photothermal conversion ability and controllable Ce6 release conferred on the nanoplatforms enhanced photodynamic therapeutic efficiency.

Chemical effects of nanoplatforms for enhanced PDT

The majority of the chemical factors that enhance the photodynamic effect are focused on overcoming the problem of hypoxia in tumor sites. Generally, nanoplatforms could load oxygen, or react with specific substances to produce oxygen in the tumor microenvironment, or produce oxygen under light stimulation.

Self-supplying oxygen nanoplatforms

In recent years, many studies have reported that various nanoplatforms, such as perfluorocarbons [134], hemoglobin [135], catalase [136], and manganese dioxide derivatives [137, 138], delivered oxygen to tumor sites to overcome anoxic environments. These substances show an improved PDT effect, and their mechanism of operation is slightly different, as explained in detail below.

Oxygen affinity nanoplatforms

Perfluorocarbons are synthetic organic molecules, typically alkanes and their derivatives, whose hydrogen atoms are replaced by fluorine atoms [139, 140]. They show biologic inertness and low toxicity even at high doses and, therefore, can be used for drug delivery. Because of the exceedingly favorable nuclear magnetic resonance properties and the virtual absence of fluorine in the human body, the perfluorocarbon carriers can also be utilized for ^{19}F magnetic resonance imaging (MRI) [141]. Furthermore, the unique electronic nature of C-F bonds endows the perfluorocarbon with excellent oxygen affinity, causing their oxygen-dissolving capacity to be much higher than that of other hydrocarbons or water and, therefore, have been widely explored for lung injury, emergency transfusion, and traumatic brain injury [142, 143]. The $^1\text{O}_2$ lifetime in perfluorocarbon (on the milli-second scale) is much longer than that in the cellular

environment or in water (on the microsecond scale). Because perfluorocarbons have high oxygen solubility and $^1\text{O}_2$ retention ability, they can maintain higher oxygen content than non-perfluorocarbon systems for potential oxygen self-enriched PDT [144-147]. As displayed in Figure 6A, Liu's group designed fluorinated covalent organic polymers by cross-linking the photosensitizer meso-5, 10, 15, 20-tetra (4-hydroxyphenyl) porphyrin with perfluorosebacic acid and PEG by a one-pot esterification [148]. The fluorinated nanoplatfoms showed efficient loading of perfluoro-15-crown-5-ether (PFCE) due to the fluorinated chains of perfluorosebacic acid. After chelating with $^{99m}\text{Tc}^{4+}$ radio-isotope utilizing the porphyrin structure of THPP, the fluorinated nanoplatfoms could be tracked by *in vivo* SPECT imaging (Figure 6B). Finally, greatly enhanced photodynamic treatment effect was observed in mice after injecting PFCE@THPP_{pf}-PEG because of the oxygen delivery by PFCE (Figure 6C). To increase the cell affinity and response of the fluorinated nanoplatfoms, Ma *et al.* developed an oxygen self-sufficient fluorinated nanoplatfom of pH-sensitive fluorocarbon-functionalized nanoparticles loaded with IR780, and used iRGD as a tumor-targeting and penetrating peptide [149]. This oxygen self-sufficient nanoplatfom could significantly enhance the tumor oxygenation and increased the generation of $^1\text{O}_2$ *in vitro* and *in vivo*. These nanoplatfoms, when injected into orthotopic breast cancer model, could remarkably inhibit the primary tumor growth and reduce lung and liver metastases. The aforementioned methods may suffer from premature oxygen release and storage issues. Furthermore, it has been reported that the stability of fluorinated nanoplatfoms is essential. To enhance the stability of the nanoplatfoms, Song *et al.* developed lipid-polymer bilaminar oxygen nanobubbles with Ce6 conjugated to the polymer shell using a combination of emulsion-solvent evaporation and internal phase separation [150]. The bilaminar shell of the nanobubbles rendered the nanobubbles biocompatible and stable. *In vitro* and *in vivo* results showed that nanobubbles exhibited much higher cellular uptake rates and tumor-targeting efficiency than free Ce6. A significant enhancement of photodynamic therapeutic efficacy was noticed due to the greatly enhanced $^1\text{O}_2$ production powered by oxygen-encapsulated nanobubbles.

Red blood cells (RBC) are the primary oxygen source of our body tissues, carrying 270 million hemoglobin molecules. Due to the binding ability of each hemoglobin for up to four O_2 molecules, RBCs have long been investigated for drug delivery. Moreover, natural RBC membranes could camouflage microparticles for successfully overcoming biological

barriers with a long blood-circulation time. Taking advantage of these properties, Wang *et al.* developed RBC hybrid nanoplatfoms, consisting of upconversion nanoparticles (UCNPs), and the rose bengal PS installation on the RBC surface [151]. Under hypoxic conditions, the inactive hypoxia probe could trigger the O_2 release from oxygenated hemoglobin under NIR excitation, further improving the PDT efficiency. Also, RBC nanoplatfoms delayed uptake by the mononuclear phagocyte system by preferentially binding to the endothelium and decreasing retention in the reticuloendothelial system. Thus, RBC nanoplatfoms show enhanced PDT under near-infrared irradiation to realize effective solid tumor eradication. Wan *et al.* prepared nanoscale RBC carriers containing sufficient oxyhemoglobin and gas-generating agent ammonium bicarbonate (ABC) for co-loading and controlled release of ICG and DOX [152]. These nanoplatfoms showed nearly identical PTT efficiency both *in vitro* and *in vivo*, but their PDT efficiency was improved significantly due to oxyhemoglobin. ABC was decomposed into NH_3 and CO_2 , further triggering the rapid release of DOX exerting cytotoxic effects. The combination of enhanced PDT and released DOX significantly inhibited breast cancer cell growth in mice and induced cell apoptosis. *In vivo* experiments confirmed that the nanoplatfoms almost completely ablated breast tumors and further suppressed tumor recurrence and metastasis.

Hemoglobin (Hb), the endogenous protein abundant in RBCs, has been used as an oxygen carrier for PDT. Compared to other carriers, hemoglobin is easily available and safe *in vivo*. However, the short circulation life, instability, and easy formation of dimers impair the treatment effect. To solve these problems, Wang *et al.* developed a hemoglobin polymer-conjugated nanoplatfom as the carrier of both oxygen and the PS to enhance PDT [153]. The amphiphilic triblock copolymer, poly (ethylene glycol) methyl ether-block-poly acrylic acid-block-polystyrene, was synthesized by atom transfer radical polymerization. The polymer and PS were covalently conjugated with Hb, and, compared with free Hb, the resulting nanoplatfom showed a high tolerance to oxidation and trypsin digestion while retaining its O_2 binding capacity. More importantly, the nanoplatfom could readily generate $^1\text{O}_2$ and kill 4T1 cells *in vitro* under light irradiation, exerting better phototoxicity with the oxygen supply of Hb. In another study, Jiang *et al.* prepared Hb-linked conjugated polymer nanoparticles, which were encapsulated in fusogenic liposomes (Hb-NPs@liposome) (Figure 7A) [154]. Due to the catalyzed activation of luminol, the conjugated poly[2-methoxy-5-(2-ethylhexyloxy)-1,4-phenylenevi

nylene] (MEH-PPV) polymer, by the oxygen supplied by Hb, the nanoparticles could acquire chemiluminescence resonance energy transfer to produce ROS. This novel system did not require an external light source and circumvented the

insufficient level of molecular oxygen for PDT. The luminescing and O₂-supplying system offers the possibility of simultaneous PDT and chemotherapy (Figure 7B).

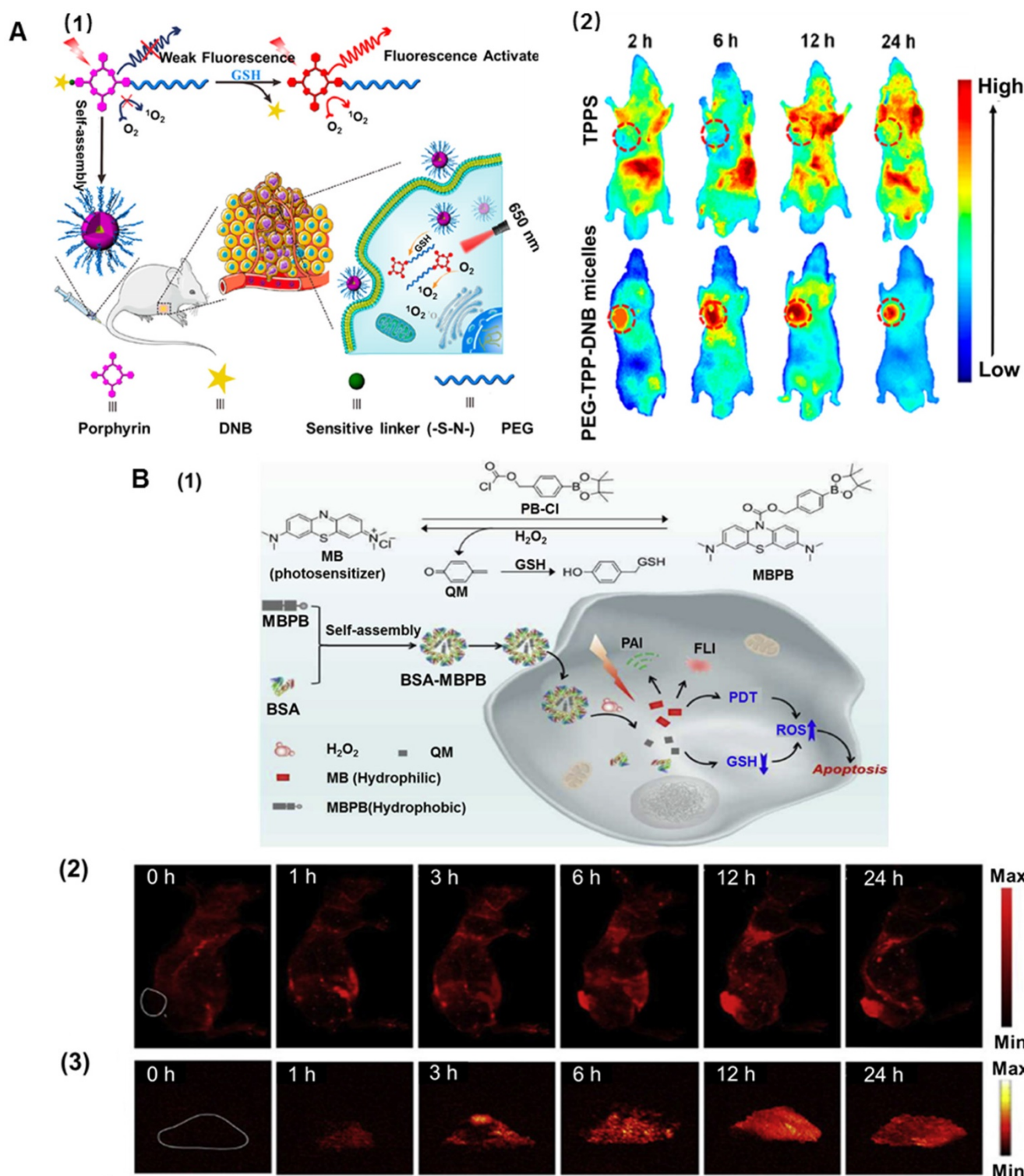


Figure 4. Redox amphiphile for enhanced PDT. Adapted with permission from ref. [102]. Copyright 2019 American Chemical Society. (1) Schematic illustration of GSH-responsive intracellular activation of amphiphilic nanoplateforms and the tumor-targeted PDT. (2) *In vivo* fluorescence imaging of the 4T1 tumor-bearing mice after intravenous injection of 5,10,15,20-tetrakis (4-sulfophenyl) porphyrin (TPPS) and PEG-TPP-DNB micelles. **B.** H₂O₂-responsive biodegradable nanomedicine for imaging-guided PDT. Adapted with permission from ref. [106]. Copyright 2019 Elsevier. (1) Schematic illustration of the synthesized photosensitizer (MBPB) and BSA-MBPB nanoplateforms, *in vivo* fluorescence (2) and photoacoustic imaging (3) before and after 1, 3, 6, 12 and 24 h post injection of nanoplateforms.

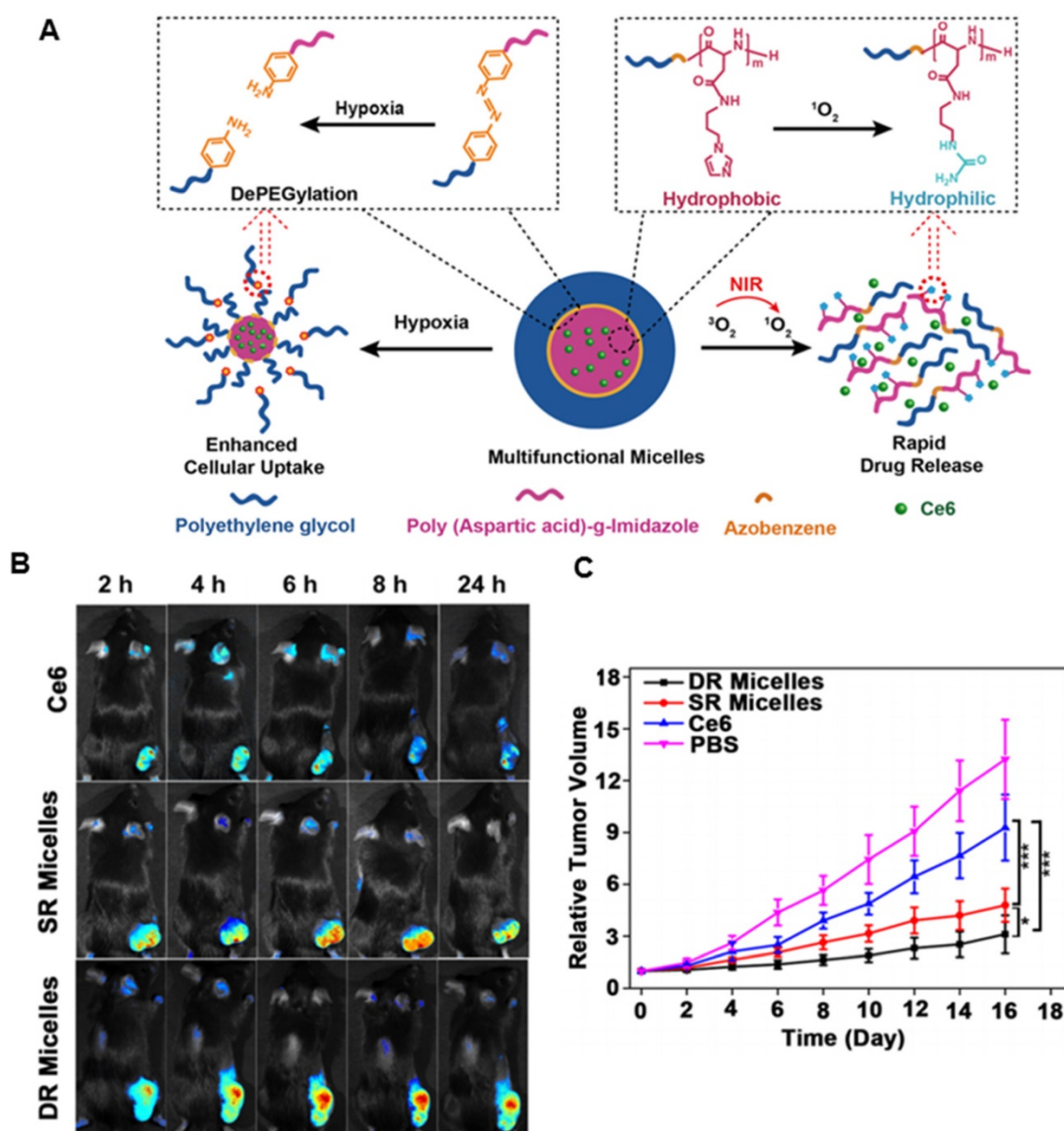


Figure 5. Polymeric micelles for enhanced PDT via interactively triggered PS delivery. **A.** Illustration of the interactively hypoxia- and singlet oxygen-sensitive tailor polymeric micelles. **B.** *In vivo* fluorescent imaging of the tumor and healthy organs up to 24 h after intravenous injection of free Ce6, Ce6-loaded SR micelles, and Ce6-loaded DR micelles. **C.** Relative tumor volume upon treatment with DR micelles and control formulations (SR micelles, free Ce6, and PBS). Adapted with permission from ref. [118]. Copyright 2018 American Chemical Society.

In situ generation of oxygen-nanoplatfoms

Catalase is a specific catalytic enzyme with an extremely high turnover to decompose H_2O_2 into O_2 and has been explored in combination with other therapeutic approaches to construct several types of nanoplatfoms to relieve tumor hypoxia [155-158]. However, after systemic administration, catalase is unstable in the presence of proteases in blood circulation. Various methods, such as encapsulation of the enzyme into inorganic nanoparticles or polymeric capsules, have been designed to protect catalase from protease digestion [159, 160]. Liu's group designed a catalase enzyme-encapsulated, Ce6-

loaded hollow silica nanoplatfom with rationally pH-responsive charge-convertible, mitochondria-targeting surface engineering [161]. Within the acidic tumor microenvironment, the nanoplatfom showed charge-conversion from negative to positive, accelerating cellular internalization and tumor retention. Also, the triphenylphosphine of this nanoplatfom could enhance PDT by targeting mitochondria. Eventually, the nanoparticles could decompose endogenous H_2O_2 in the tumor and alleviate tumor hypoxia, greatly enhancing PDT treatment of solid tumors. Furthermore, the nanoparticles showed synergistic effects when combined with anti-PD-L1 checkpoint blockade to

induce robust antitumor immunity, which could suppress tumor growth without direct light exposure. Subsequently, his group also loaded catalase into the capsule by in situ free-radical polymerization, using double-bonded meso-tetra(phydroxyphenyl) porphine as the cross-linker to enable condensed grafting of short polyethylene glycol chains on the protein surface as a permeable brush-like safeguard [162]. The catalase-entrapped nanocapsules exhibited efficient passive retention in tumors after intravenous injection, which could significantly overcome tumor hypoxia by triggering the decomposition of endogenous tumor H_2O_2 into oxygen, achieving a remarkable antitumor therapeutic effect. Also, the nanocapsules showed greatly prolonged blood circulation, with the blood half-life of ≈ 6.42 h and effective tumor accumulation of $6.03 \pm 1.78\%$ ID g^{-1} . However, it was reported that the relative enzymatic activity of catalase-encapsulated nanocarriers might

decrease during the synthetic processes. To tackle the issue, Zhao's group developed therapeutic nanoplatfoms consisting of catalase-encapsulated β -cyclodextrin-HA nanoparticles loaded with adamantane-modified Ce6 by supramolecular means (Figure 8A) [163]. The obtained therapeutic nanoplatfom could target overly expressed CD44 receptors on MDA-MB-231 cells, where the encapsulated catalase could decompose the endogenous H_2O_2 to generate O_2 for alleviating hypoxia in cells incubated under hypoxic conditions. The nanoplatfom also exhibited high cellular cytotoxicity under hypoxic condition because of the ability of catalase in mitigating hypoxia. *In vivo* experiments revealed that the tumor growth from group V was the most inhibited one among all groups, illustrating the highest antitumor efficacy of HA-CAT@aCe6 (Figure 8B and 8C).

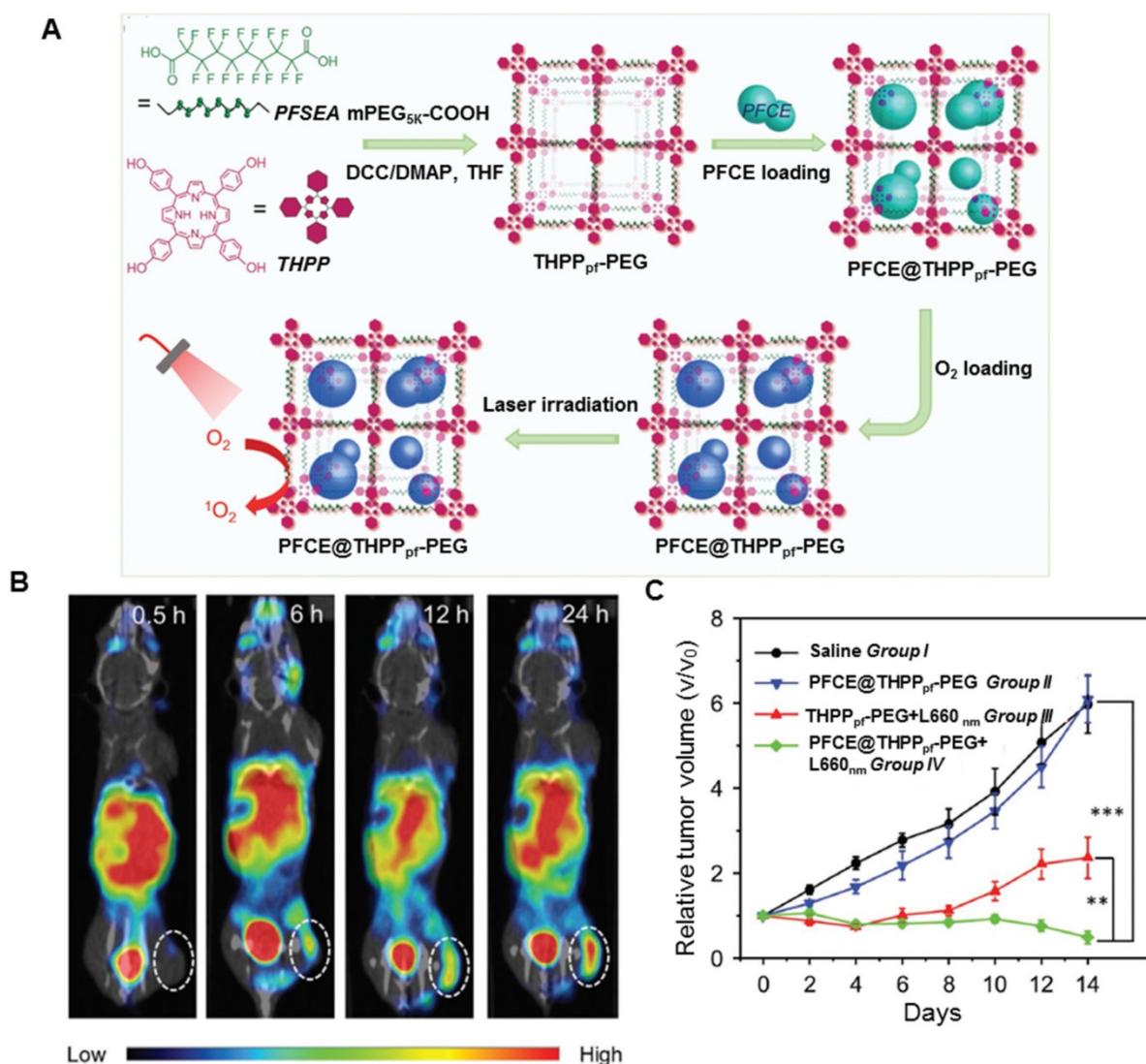


Figure 6. Covalent organic polymers for enhanced PDT. **A.** Scheme illustrating the synthesis route of THPP_{pr}-PEG and the subsequent PFCE loading. **B.** SPECT images of 4T1 tumor-bearing mice with the injection of PFCE@THPP_{pr}-PEG recorded at different time intervals. **C.** Tumor growth curves of four groups of mice after treatments as indicated. Adapted with permission from ref. [148]. Copyright 2018 Wiley-VCH.

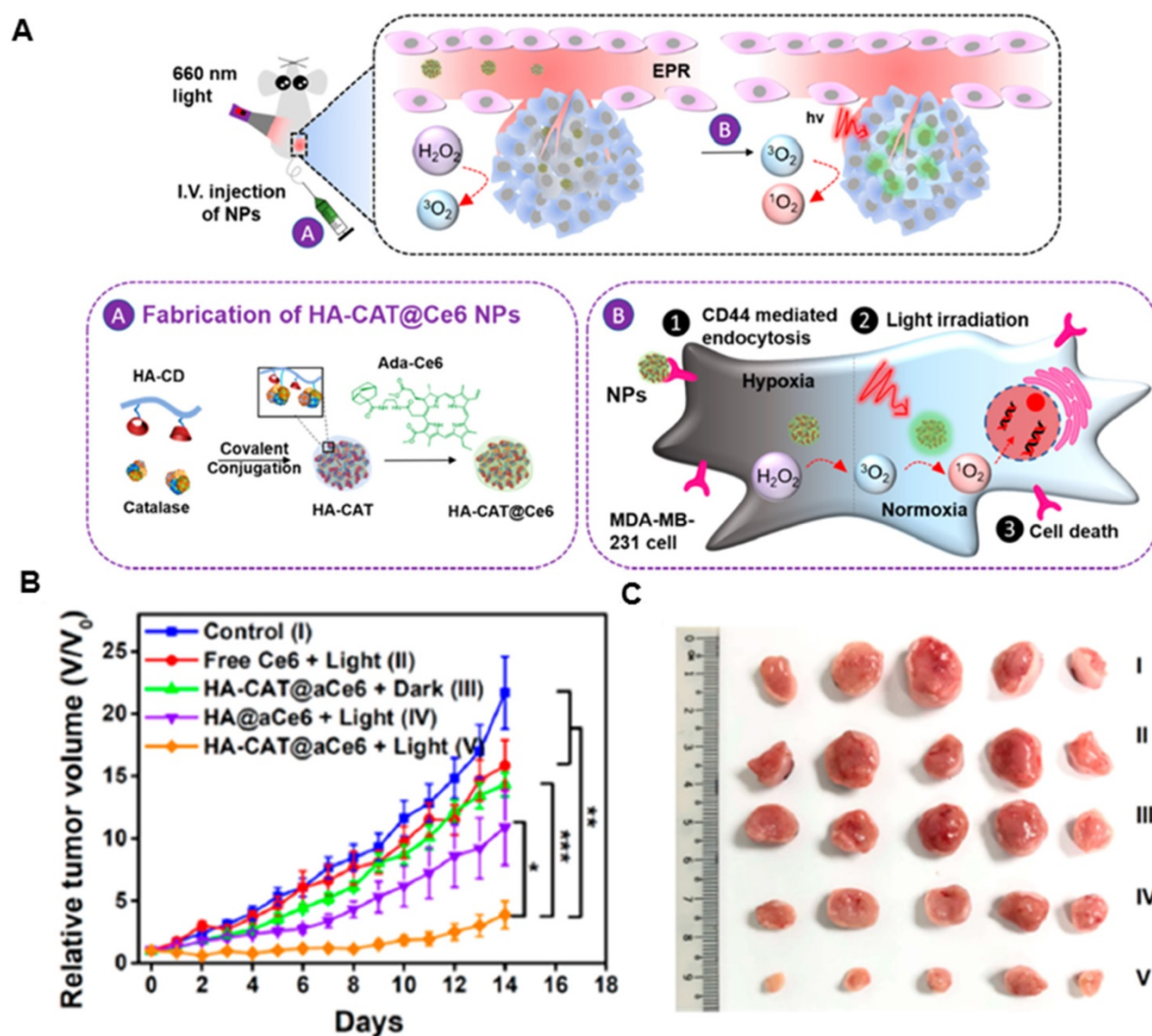


Figure 8. Catalase-integrated hyaluronic acid for enhanced PDT. **A.** Schematic illustration of the processes after intravenous injection of HA-CAT@aCe6 nanoplatforms into tumor-bearing mice. **B.** Relative tumor volumes of MDA-MB-231 tumor bearing mice with five treatment groups over 14 days. **C.** Photos of excised tumors from mice on the 14th day after these treatments. Adapted with permission from ref. [163]. Copyright 2019 American Chemical Society.

Despite the use of MnO_2 nanoparticles to generate O_2 or consume GSH in the tumor microenvironment, several limitations, including rapid consumption of MnO_2 , transient O_2 generation or GSH depletion, hamper the efficient regulation of tumor hypoxia and fail to continuously and synchronously enhance ROS-based therapeutic effect [177]. Overcoming these drawbacks requires the development of a persistent strategy to regulate tumor microenvironment. To enhance PDT efficiency, Kim *et al.* developed biocompatible manganese ferrite nanoparticles anchored onto mesoporous silica nanoparticles [178]. Exploiting the continuous generation of oxygen by $MnFe_2O_4$ nanoparticles through the Fenton reaction under physiological conditions, the nanoplatform could enhance ROS generation of PS, thus improving the therapeutic

outcome of PDT for tumors *in vivo*. Furthermore, these nanoplatforms exhibited T_2 contrast effect in MRI, allowing *in vivo* tracking of nanoplatforms. Based on previous findings, Zhang *et al.* developed biocompatible nanoplatforms by concentrating a coating of porphyrin-based MOF as the PS and $MnFe_2O_4$ as the nanoenzyme (Figure 10A) [179]. The $MnFe_2O_4$ @MOF nanoplatform exhibited both catalase and glutathione peroxidase-like activities. Once internalized in the tumor, the nanoparticles could continuously catalyze H_2O_2 to produce O_2 by cyclic Fenton reaction and also persistently reduce GSH in the presence of H_2O_2 , decreasing the depletion of ROS upon laser irradiation during PDT. $MnFe_2O_4$ @MOF was also used for MRI-guided precision cancer therapy (Figure 10B). An enhanced photodynamic therapeutic effect arose from simultaneously self-

producing O_2 and self-decreasing GSH (Figure 10C).

Besides MnO_2 carriers for PDT, hybrid nanoplatforms assembled from MnO_2 and other nanomaterials are sometimes more effective in enhancing PDT. Bhattacharyya *et al.* developed unique two-dimensional hybrid nanoplatforms based on PEGylation of MnO_2 -decorated p-MoS₂/n-rGO heterojunction nanosheets [180]. The resulting nanoplatforms showed better biocompatibility and colloidal stability in physiological solutions. The p-n heterojunction directed NIR-triggered generation and separation of electron-hole pairs, which improved the production of ROS via photocatalysis. Also, MnO_2 increased intracellular O_2 by reacting with endogenous H_2O_2 in the cellular microenvironment. The hybrid nanoplatforms have been demonstrated as

PDT-enhanced agents for cancer therapy. In another study, Wang *et al.* developed a chemo-photodynamic nanoplatform (FMZ/DC) by one-pot encapsulation of g-C₃N₄ and DOX in ZIF-8, then loading MnO_2 nanodots and surface-modifying F127 (Figure 11A) [181]. The hybrid nanoplatforms could generate oxygen upon the addition of H_2O_2 , further demonstrating the enhanced therapeutic effects for both chemotherapy and PDT therapy. *In vivo* tumors treated with FMZ/DC began to shrink after 2 days of chemo-photodynamic therapy. The outstanding therapeutic effect could be ascribed to the oxygen-generating ability of the nanoplatform, improving the efficiency of photodynamic and chemotherapeutic treatments (Figure 11B and 11C).

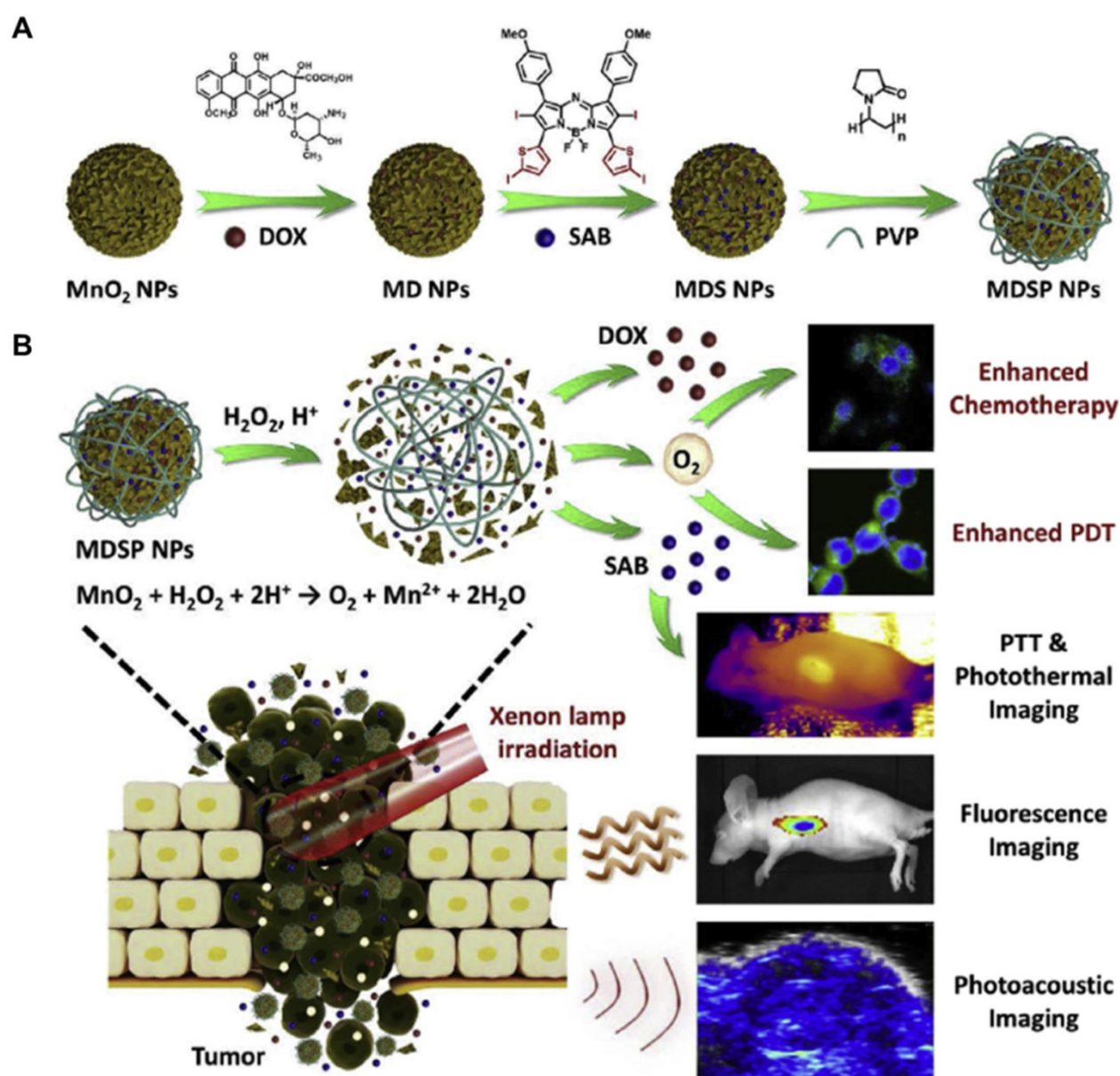


Figure 9. Hydrangea-structured nanoplatforms for tumor imaging and therapy. **A.** Schematic illustration of the fabrication of MDSP NPs. **B.** MDSP NPs for tumor microenvironment responsive chemo/photodynamic/photothermal therapy under xenon lamp irradiation. Adapted with permission from ref. [175]. Copyright 2019 Elsevier.

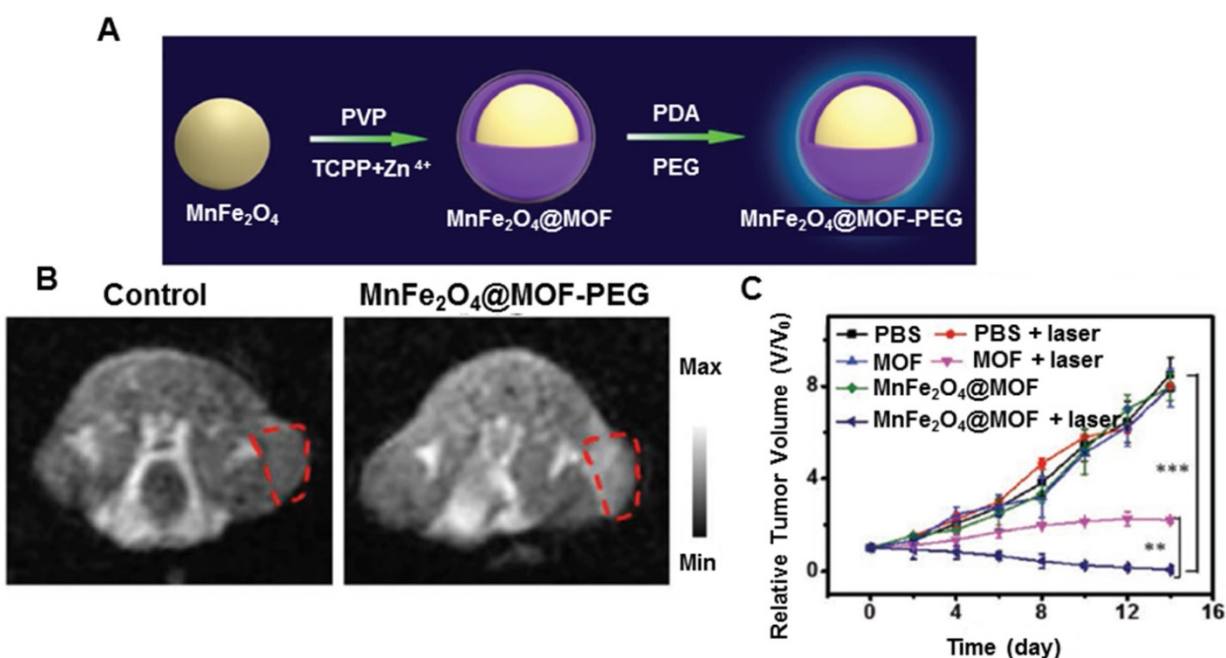


Figure 10. MnFe_2O_4 @metal-organic frameworks for enhanced PDT. **A.** Schematic illustration of the synthesis process of MnFe_2O_4 @MOF core-shell nanostructure. **B.** *In vivo* T_1 -weighted MR images of mice at 24 h post injection of PBS or MnFe_2O_4 @MOF-PEG. **C.** Tumor growth curves of each group post-intratumoral administration under laser irradiation. Adapted with permission from ref. [179]. Copyright 2019 Wiley-VCH.

Encouraged by the excellent catalytic performance of natural enzymes, varieties of synthetic structures have been designed to mimic the functions and complexities of natural enzymes over the past few decades. Various artificial nanozymes are emerging and attracting extensive research interest [182, 183]. Platinum nanoparticles are well-known catalysts for many chemical reactions, whose enzyme mimetic activities have been reported previously [184]. As illustrated in Figure 12A, Zhang *et al.* developed a porphyrinic Zr-MOF derived from PS and Zr in which Pt nanoparticles were homogeneously decorated on MOF via an *in-situ* reduction and further coated with PEG to greatly improve the biocompatibility and physiological stability [185]. The obtained nanoplatform with high catalase-like activity induced the decomposition of H_2O_2 to produce O_2 at the hypoxic tumor site, facilitating the formation of cytotoxic $^1\text{O}_2$ to kill cells. The tumor growth was completely inhibited when the mice were injected with the nanoplatform (PCN-224) after irradiation treatment (Figure 12B and 12C). Thus, the nanoplatform exhibited much improved PDT efficiency via H_2O_2 -activated generation of O_2 and light-irradiated formation of $^1\text{O}_2$. Similarly, Wei *et al.* designed Pd@Pt bimetallic nanoplates, which were further covalently conjugated with Ce6 and bifunctional PEG [186]. The nanoplatform could produce O_2 over a long period by reacting with H_2O_2 in the tumor sites. Also, the moderate photothermal effect of the nanoplatform under 808 nm laser irradiation could further improve the PDT efficacy in

hypoxic tumors by accelerating its catalytic decomposition of H_2O_2 . Both *in vitro* and *in vivo* results indicated that the nanoplatform effectively delivered PS to cancer cells/tumor sites and triggered the decomposition of endogenous H_2O_2 to generate oxygen, resulting in a remarkably enhanced PDT efficacy.

Other nanoplatforms for generating oxygen

Besides the nanoplatforms mentioned earlier, oxygen bonding and *in situ* generation of oxygen, some researchers have attempted to endow nanoplatforms with oxygen by other means to enhance PDT. Wang *et al.* developed core-shell nanoparticles based on a double emulsion method, wherein the H_2O_2 / poly(vinylpyrrolidone) complex and poly(lactic-co-glycolic acid) (PLGA) served as the core and shell, respectively. The hydrophilic H_2O_2 / poly(vinylpyrrolidone) complex acted as an oxygen source, while hydrophobic IR780 was the PTT/PDT agent. When the resultant nanoplatforms were internalized by HepG2 cells, they could generate the photothermal effect where ROS was released to kill cancer cells under an 808 nm laser irradiation. Moreover, the encapsulated H_2O_2 could supply additional oxygen and, in turn, significantly enhance the PDT effect [187]. The nanoplatforms accumulated in the xenograft tumor and could inhibit tumor growth due to combinational PTT and enhanced PDT upon NIR light irradiation. Xie *et al.* developed an O_2 -loaded pH-responsive multifunctional nanoplatform (UC@mSiO₂-RB@ZIF-O₂-DOX-PEGFA) with

enhanced chemo-photodynamic therapeutic effect [188]. $\text{NaYF}_4:\text{Yb}/\text{Er}@\text{NaYF}_4:\text{Nd}@\text{NaGdF}_4$ nanoparticles were employed as both upconversion/MRI matrix and motivator for rose red PS in PDT with deep penetration depth. Zeolitic imidazolate framework-90 was capped outside of mSiO_2 as an O_2 reservoir to quickly release O_2 in the tumor microenvironment, thereby improving the PDT efficiency. Additionally, DOX and NH_2 -poly(ethylene glycol)-modified folic acid were covalently adsorbed on the surface of nanoparticles for synergetic therapy. Li *et al.* developed upconversion nanophotosensitizers with hyperbaric oxygen (HBO) to change the extracellular matrix for enhanced photodynamic

cancer therapy [189]. The UCNPs were developed for Nd^{3+} -sensitized sandwiched structure, wherein the upconversion core served as a light transducer to transfer energy to the neighboring rose bengal to produce ROS. With HBO, the photodynamic process could induce abundant ROS in the intrinsically hypoxic tumor. Furthermore, HBO-assisted PDT decomposed collagen in the extracellular matrix of tumors and facilitated the diffusion of oxygen and penetration of nanoplatforms into the deeper area of the tumor. Such a synergic effect eventually caused enhanced therapeutic efficacy at a low laser power density as compared with those using UCNPs alone.

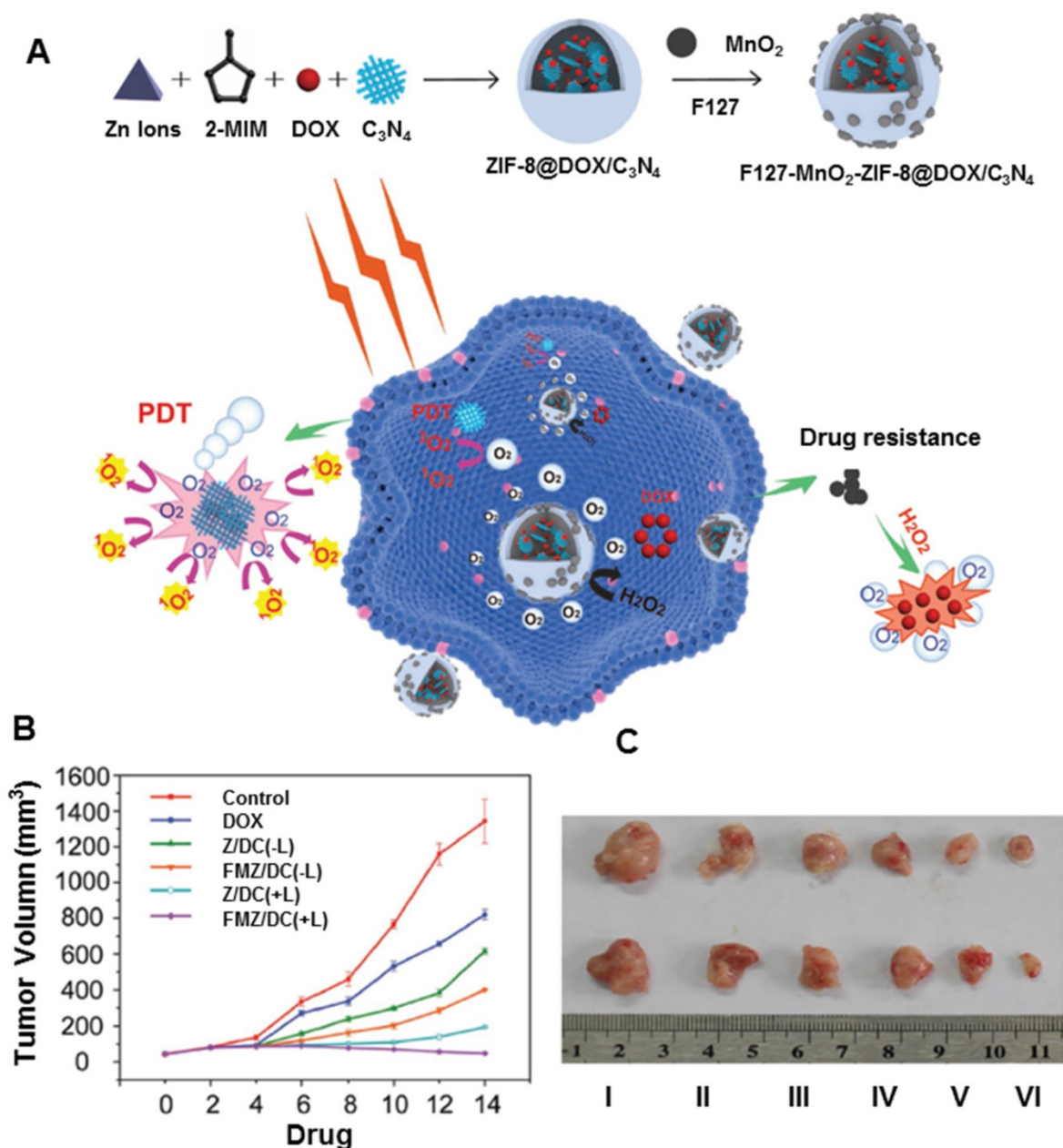


Figure 11. MnO_2 nanodots-anchored nanoplatforms for chemo-PDT. **A.** Schematic illustration of the fabrication of FMZ/DC nanoplatforms with oxygen generation enhancing the chemo-photodynamic therapy. **B.** Tumor growth curves of different groups of 4T1 tumor-bearing mice. **C.** Images of tumors collected from different groups of mice 14 day after different treatment. Adapted with permission from ref. [181]. Copyright 2018 Wiley-VCH.

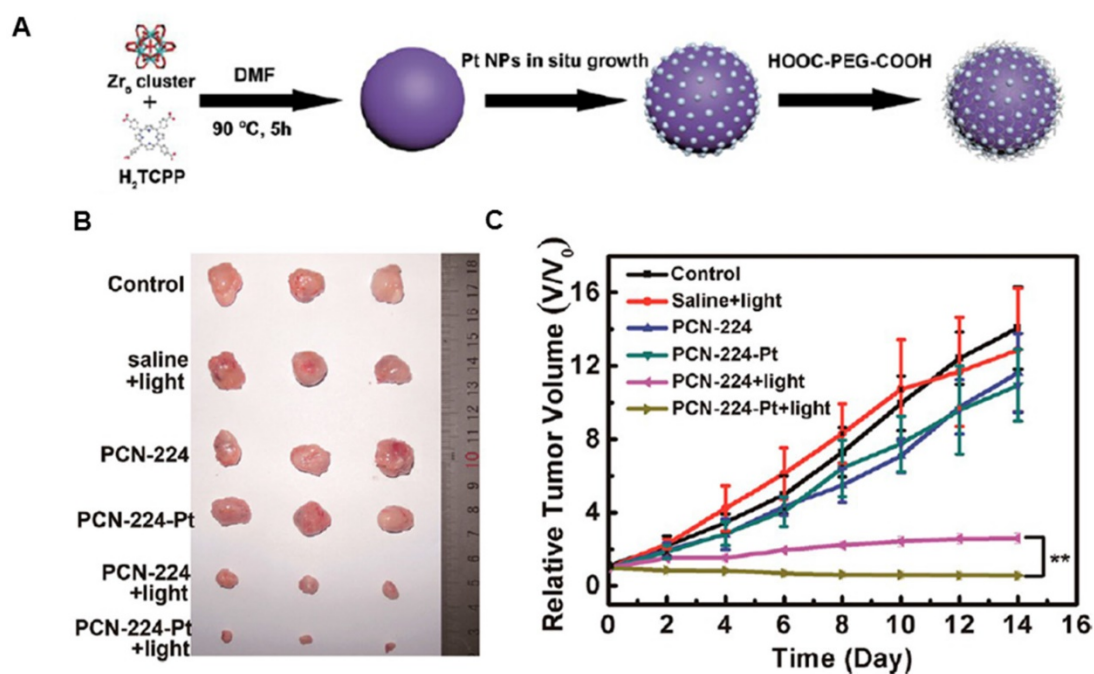


Figure 12. Nanozyme decorated MOF for enhanced PDT. **A.** Schematic illustration of the preparation process of PCN-224-Pt. **B.** Representative photographs of the tumor dissection. **C.** Relative tumor volume after various treatments indicated. Adapted with permission from ref. [185]. Copyright 2018 American Chemical Society.

Water-splitting materials

Due to possibly worsening hypoxia, the PDT may cause irreversible tumor metastasis or drug resistance. Highly efficient production of O₂ can potentially compensate for the tumor hypoxic microenvironment. Compared to the aforementioned nanoplatforms able to produce oxygen, water is the most abundant compound in the physiological environment [190] and could provide unlimited raw material for O₂ generation. To date, a variety of splitting materials have been innovatively constructed to generate oxygen and hydrogen for clean, renewable resources, also extending the strategy to PDT [191]. The commonly used water-splitting nanoplatforms include oxides (titanium dioxide), carbon or nitrogen compounds (carbon nitride and MXene), and sulfides.

Titanium dioxide (TiO₂) has received considerable attention for its adjustable band gap, band position, superior photostability, high intrinsic catalytic activity, abundance, low toxicity, and inexpensiveness [192-194]. Yang *et al* developed carbon-nanodot-decorated TiO₂ nanotubes as a nanoplatform for PDT [195]. In this formulation, carbon dots (CDots) could increase the light absorption response and narrow the band-gap compared with anatase TiO₂ nanoparticles. Interestingly, CDots/TiO₂ nanotubes could absorb the 650 nm NIR light, where the emission wavelengths (325-425 nm) of CDots excite TiO₂ nanotubes to form electron/hole (e⁻/h⁺) pairs, inducing the reaction with the adsorbed oxidants to produce ROS. Besides, the

CDots showed high chemical catalytic activity for H₂O₂ decomposition. The excellent PDT performance actuated by 650 nm light was verified by *in vivo* assays. Using an organometallic ruthenium complex (N₃) as a conjugator, Gilson *et al* prepared TiO₂-N₃ nanoplatforms [196]. Upon exposure of TiO₂-N₃ to light, N₃ injected electrons into TiO₂ to produce three- and four-fold hydroxyl radicals and hydrogen peroxide. Furthermore, the inability of TiO₂ to produce H₂O₂ under hypoxic conditions suggested that N₃ facilitated the depletion of residual H₂O₂ and rapid conversion of the low oxygen concentration into •OH, thus increasing the concentration of this species. TiO₂-N₃ maintained three-fold higher hydroxyl radicals than TiO₂ under hypoxic conditions via N₃-facilitated electron-hole reduction of adsorbed water molecules. These results demonstrated a mechanism to convert and maintain cytotoxic •OH production by harnessing the reductive power of ruthenium complexes, which efficiently reduced low levels of oxygen for ROS production.

Carbon nitride (C₃N₄) has received considerable attention for the adjustable band gap and band position [197, 198]. After the modification, water splitting can be driven under high penetrable red light >600 nm, which makes C₃N₄ suitable for *in vivo* therapy. Most importantly, due to the absence of metal elements, C₃N₄ is thought to be a highly biocompatible material for biomedical applications. As presented in Figure 13A, Zheng *et al.* developed CDots-doped C₃N₄ nanoparticles, and further modified with an amphipathic polymer (PpIX-PEG-

RGD) [199]. The as-prepared nanoplatform could split water to generate O_2 under 630 nm laser radiation with high efficiency. The PS could further transmit the energy to the produced O_2 to generate cytotoxic 1O_2 . *In vitro* study showed the nanoplatform could increase the intracellular O_2 concentration and improve the ROS generation in both hypoxic and normoxic environments. After the injection, PpIX fluorescence started to accumulate in the tumor (Figure 13B). The *in vivo* experiment indicated that CDots-doped C_3N_4 (CCN) nanoparticles and PpIX showed little inhibitory effects on 4T1 tumors. However, treatment with polymer-modified, CDots-doped carbon nitride nanoparticles (PCCN) exhibited remarkable growth inhibition against tumors with only one injection (Figure 13C and 13D), which could be attributed to its tumor targeting and O_2 generation. Recent studies also reported that metal ion-doped C_3N_4 nanoplatforms showed better-enhanced PDT. Jiang *et al.* developed the fusiform Fe^{III} -doped C_3N_4 nanoplatform, further modified by mitochondria-targeting molecular (4-carboxybutyl) triphenyl-phosphonium bromide (TPP) [200]. The ultrahigh surface area of the nanoplatform enhanced the

loading capacity of methylene blue, while mitochondria-targeting TPP agent improved the ROS concentration, thus accelerating the mitochondrion dysfunction and further triggering cell death during PDT. The doping of Fe^{III} showed excellent catalytic performance towards H_2O_2 in cancer cells to generate O_2 , thus overcoming tumor hypoxia and enhancing the PDT efficacy. In addition, the introduction of Fe^{III} endowed the Fe^{III} -doped C_3N_4 nanoplatform with an effective T_1 -weighted MRI contrast ability for simultaneous imaging and therapy. Likewise, Qu *et al.* reported that the combination of Cu^{2+} and $g-C_3N_4$ nanosheets (Cu^{2+} - $g-C_3N_4$) led to increased light-triggered ROS generation as well as the depletion of intracellular GSH levels [201]. Consequently, the ROS generated under light irradiation could be depleted less by reduced GSH, thus improving efficiency. Importantly, Cu^{2+} - $g-C_3N_4$ nanosheets could catalyze the reduction of molecular oxygen to the superoxide anion or hydrogen peroxide to the hydroxyl radical, both of which accelerated the generation of ROS. This synergy of improved ROS generation and GSH depletion could enhance the efficiency of PDT for cancer therapy.

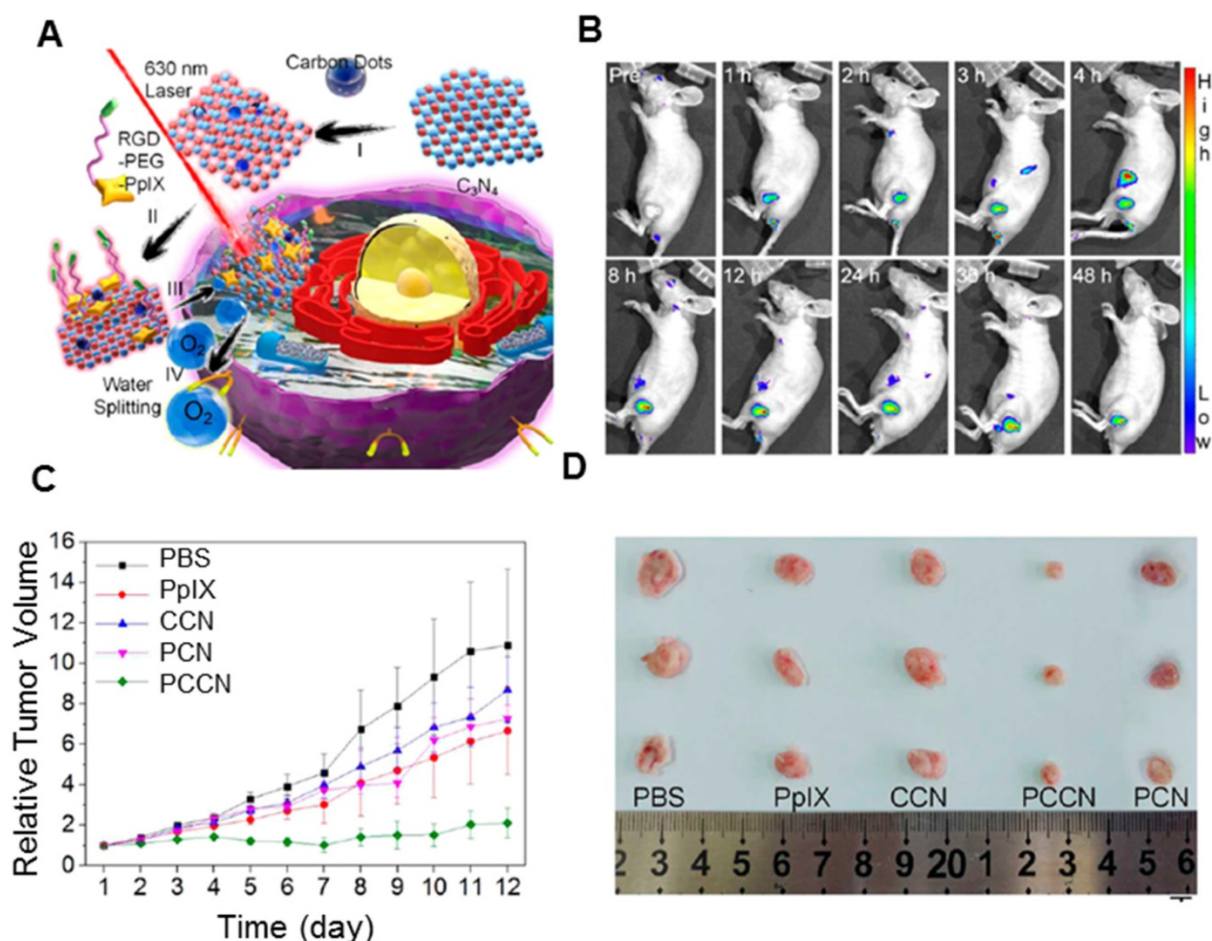


Figure 13. A. Structure of PCCN and schematic diagram of 630 nm light-driven water splitting enhanced PDT. B. *In vivo* fluorescence imaging of PCCN at different time points after intravenous injection. C. Tumor images at the 12th day post-treatment. D. Relative tumor volume post-treatment, the intravenous injection of samples was performed on different days. Adapted with permission from ref. [199]. Copyright 2016 American Chemical Society.

Wang *et al.* developed a biomimetic ultrathin graphdiyne oxide from oxidized and exfoliated graphdiyne, which was further modified by iRGD peptide-modified RBC membrane [202]. The obtained nanoplatform showed prolonged blood circulation via RBC membrane camouflage along with enhanced extravascular and hypoxic region penetration by a functional iRGD peptide. The nanoparticles could efficiently catalyze water oxidation to release O₂ and generate ¹O₂ using 660 nm irradiation. More importantly, the hyperthermia effect of ultrathin graphdiyne oxide could conveniently cause dilation of vessels and blood perfusion for overcoming perfusion-limited hypoxia. Consequently, with O₂ evolving from photocatalysis water splitting together with blood perfusion from photothermal conversion, this nanoplatform alleviated diffusion- and perfusion-limited hypoxia synchronously and further enhanced PDT.

The above-mentioned results indicated that numerous materials could improve intratumoral O₂ and ROS supplementation for enhanced PDT (Table 2). However, the limited O₂ binding sites in Hb and low solubility of O₂ in perfluorocarbon restricted the efficacy. Additionally, the low intracellular concentration of H₂O₂ significantly limited the O₂ production yield and thus achieved only moderate efficacy in cancer therapy. As the most abundant compound in living organisms, water provides enough O₂ for *in vivo* PDT. Therefore, the construction of highly catalytic nanoplatforms is essential for PDT.

Physical effects of nanoplatforms for enhanced PDT

The efficiency of PDT is also affected by physical factors, such as light sources [203], magnetic field [204], electric fields [205], microwaves [206], and ultrasound [207]. Compared with light, the microwave is a superior energy source to trigger the ROS generation for tumor therapy. However, microwave energy is considered to be insufficient for inducing free radical generation, making microwave dynamic therapy subject to certain restrictions [208]. Ultrasound can activate PS for tumor cell destruction useful for penetrating deep tissues. This novel approach is known as sonodynamic therapy [209]. Some studies have shown that the efficiency of ultrasound-activated PS needs to be further improved. The microwave of the electromagnetic spectrum has been extensively explored for tumor ablation in clinical settings, especially microwave thermal therapy because of the penetration depth in tissues, high heating efficiency, and negligible side effects. Magnetic nanoparticles are promising candidates for controlled drug delivery, hyperthermia

therapy, and MRI [210]. When subjected to oscillating magnetic fields, the magnetic nanoplatforms could generate heat for targeted tumor therapy. Moreover, magnetic nanoplatforms can absorb NIR light to induce hyperthermia. Therefore, a combination of magnetic nanoparticles and the PS in nanoplatforms leads to enhanced PDT efficacy. Some physical effects to enhance PDT are summarized in the Table 3.

X-rays nanoplatforms

Most of the solid tumors are located several millimeters under human skin, whereas, the penetration depth of UV/visible light into biological tissues is merely several micrometers [211]. Such limited penetration depth results in low tumor-killing efficiency. Many efforts have been devoted toward the development of the novel nanoplatforms to surmount the challenges from such poor and limited light tissue penetration. These nanoplatforms, on the one hand, involve the introduction of enhanced chemi- or bioluminescent probes as well as multiphoton and upconverting materials. On the other hand, they utilize external ionizing radiation to penetrate deep into the human body as a neoadjuvant treatment. As is widely accepted, X-rays exhibit a high penetration depth in the human body for clinical imaging. It holds the potential to become an ideal excitation source for activating PS accumulated in deep tumor tissue [212, 213]. In a typical X-rays assisted PDT, the absorbed X-ray energy was converted into photons with the appropriate wavelength, which were further absorbed effectively by PS. The resultant ROS from PS could directly damage the tumor cells, and the absorbed ionizing radiation could also generate radical species and break DNA double-strands [214, 215]. To match the energy difference between X-rays (keV-MeV) and the light absorbed by PS (eV), lanthanide-based scintillators and heavy metals have been adopted to absorb X-rays and transmit the energy to PS, leading to efficient luminescence in the visible light region. Since Tb³⁺ shows efficient green luminescence that matches well with the absorption band of porphyrin. Chen's group synthesized water-soluble LaF₃:Tb³⁺-porphyrin conjugates to study ¹O₂ generation under X-rays irradiation. Anthracenedipropionic acid (ADPA) was used to measure the ¹O₂ generated by the porphyrin and LaF₃:Tb³⁺-porphyrin conjugates. Upon X-rays irradiation, the luminescence of ADPA quenched much faster in LaF₃:Tb³⁺-porphyrin conjugates than in the porphyrin solution. Therefore, high production of ¹O₂ in the LaF₃:Tb³⁺-porphyrin conjugates was verified because of the energy transfer from the LaF₃:Tb³⁺ nanoparticles to porphyrin [216]. Similarly, mesoporous LaF₃:Tb³⁺ nanoparticles were proposed to load rose

bengal for establishing an efficient fluorescence resonance energy transfer system [217]. These results indicated that a large amount of $^1\text{O}_2$ could be generated in X-rays PDT for deep-seated tumor treatment. Moreover, recent years have witnessed the development of *in vivo* applications of X-rays PDT. Wang *et al* developed hybrid nanoplatforms based on $\text{LiLuF}_4:\text{Ce}@\text{SiO}_2@\text{Ag}_3\text{PO}_4@\text{Pt(IV)}$ to enhance the curative effects of X-rays PDT (Figure 14). $\text{LiLuF}_4:\text{Ce}$ nanoparticles were employed as the scintillator, and a cisplatin prodrug Pt(IV) was used as a sacrificial electron acceptor to increase the yield of hydroxyl radicals by boosting the separation of electrons and holes in Ag_3PO_4 . Cisplatin was produced when Pt(IV) accepted electrons, which could damage the deoxyribonucleic acid in cancer cells, thereby enhancing the effect of X-rays PDT [218]. To endow X-rays PDT with diagnosis information, enriched scintillation nanoparticles ($\text{CeF}_3:\text{Gd}^{3+},\text{Tb}^{3+}$), coated with mesoporous silica for loading rose bengal, were developed in the treatment of deep-seated tumors [219]. The results showed an efficient tumor regression with synergistic nonradioactive radio-/photodynamic therapy under the guidance of computed tomography (CT) and MRI *in vivo*. Besides, other nanoplatforms of mesoporous silica-coated gold nanorods with conjugated europium (Eu) complexes were proposed for photothermal and X-rays PDT. Europium (Eu) complexes efficiently transfer the X-rays energy to hematoporphyrin for PDT treatment. *In vitro* and *in vivo* studies indicated that nanoplatforms showed CT and photoacoustic imaging for deep tumor penetration. An effective suppression of tumor progression was verified under X-rays and laser irradiation *in vivo* [220]. Besides, QDs-based, silicon-based, and metal-based nanoscintillator have also been proposed and studied [221]. In view of size-dependent photoluminescence of QDs and silicon semiconductor nanoparticles, their absorbance and photoluminescence could easily be adjusted for PDT. Moreover, they showed well biodistribution properties and could be eliminated from the body in a relatively short time. Remarkably, QDs could transfer energy to a molecular PS or directly to molecular O_2 , both of which can generate $^1\text{O}_2$ for X-rays PDT. As metal-based nanoscintillators, gold nanoparticles exhibited excellent absorbers of X-rays and have been studied as radiosensitizers for radiotherapy. Deng and co-authors developed novel mitochondria targeted PLGA-based nanoplatforms containing ultrasmall gold nanoparticles and verteporfin. The nanoplatforms demonstrated a higher ability to generate $^1\text{O}_2$ compared to PLGA-loaded verteporfin. Furthermore, they produced a large amount of $^1\text{O}_2$ within the mitochondria *in vitro*

upon X-rays radiation, thus triggering mitochondria-related apoptosis of cancer cells. Obviously inhibited growth of *in vivo* tumor with only a fraction of radiotherapy dose by X-rays PDT [222]. Despite some progress have been made, some *in vivo* studies are conducted by intratumoral injection of nanoplatforms, which is ineffective to the non-invasive clinical treatment of deep-seated tumor due to poor specificity upon their uptake in these cancer cells. What's more, the interplay between PDT and ionizing irradiation remain unclear, and the low-dose irradiation, energy conversion as well as safety profiles need further explorations.

Surface plasmon resonance of nanoplatforms

The electromagnetic-near-field enhancement mechanism of plasmonic nanoparticles has been exploited to control $^1\text{O}_2$ generation. When the localized surface plasmon resonance (SPR) band was close to the absorption band of nearby PS, the absorption coefficient of PS could be significantly improved by the localized electric field, thereby increasing the production efficiency of ROS [223, 224]. So far, plasmonic gold-based nanoplatforms have been explored to enhance the $^1\text{O}_2$ by strong and tunable SPR. Li *et al.* developed a nanoplatform composed of mesoporous silica-coated gold nanorods incorporating indocyanine green [225]. The SPR of gold nanorods was regulated to overlap with ICG exciton absorption. Such an overlap greatly increased the $^1\text{O}_2$ yield of incorporated ICG under laser excitation. Furthermore, the nanoplatform possessed a synergistic PTT effect based on both Au nanorod and ICG. The integrated strategy significantly improved photodynamic destruction of breast tumor cells and inhibited the growth of orthotopic breast tumors in mice through the synergistic effect of PDT and PTT. To exploit the SPR advantages of gold nanorods, the nanoplatform consisting of $\text{NaYF}_4:\text{Yb}/\text{Er}$ conjugated with gold nanorods was prepared to boost the therapeutic efficiency of PDT [226]. Methylene blue was embedded inside the silica shell to increase photostability and prevent drug leakage. UCNPs could convert NIR light to visible light to excite methylene blue for the generation of ROS. More importantly, gold nanorods could effectively increase upconversion efficiency and ROS content through a localized SPR effect. The mechanism of plasmon-enhanced PDT was verified by enhancing upconversion luminescence intensity through the plasmonic field and by increasing the light-harvesting capability and absorption cross-section of the system. Consequently, the nanoplatform could produce ROS and undergo efficient PDT *in vitro* and *in vivo*. The plasmonic Au nanoparticles integrated with the black

phosphorus nanosheet simultaneously enhanced the ¹O₂ generation and hyperthermia by localized SPR effects for cancer phototherapy [227]. The hybrid nanoplatform not only significantly increased 3.9-fold ¹O₂ production of black phosphorus nanosheet, but also achieved 1.7-fold increase in photothermal conversion efficiency upon single laser irradiation

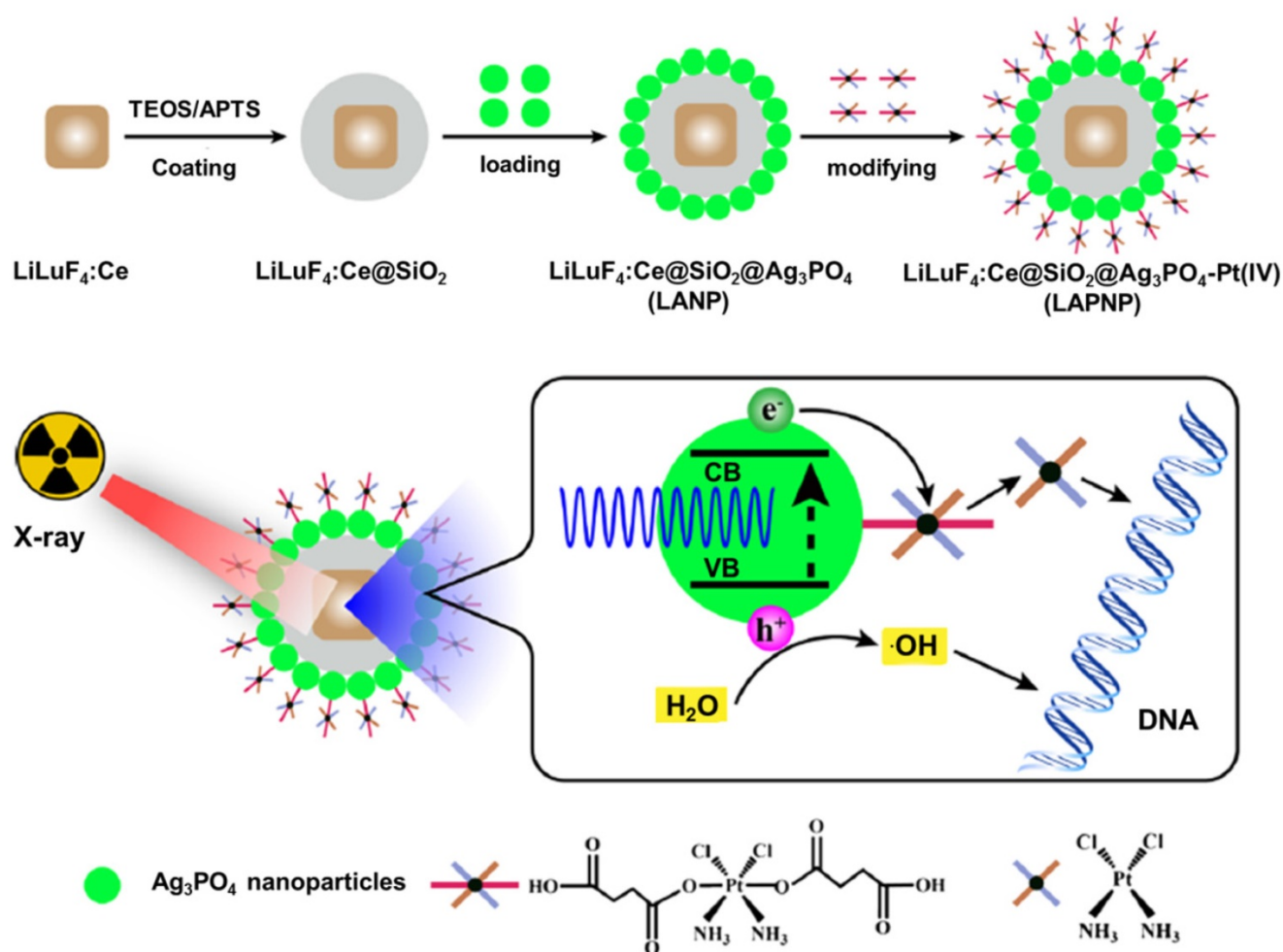
with 670 nm. When mice were subjected to laser irradiation, the nanoplatform showed stronger inhibition of tumor growth than other controls. The nanoplatform could almost completely restrain the tumor growth over 14 days due to enhanced PDT/PTT synergistic therapeutic effects.

Table 2. Chemical effects of nanoplatforms for enhanced PDT

Nanoplatforms design	PS	Enhanced mechanism	Improved therapeutics	Ref
Perfluorotributylamine-HSA	IR780	Perfluorotributylamine affinity O ₂	PDT	146
Perfluorohexane @Ce6@O ₂ nanodroplets	Ce6	Perfluorohexane affinity O ₂	PDT	147
Covalent organic polymers with PFC	Porphyrin	Perfluoro-15-crown-5-ether affinity O ₂	PDT	148
Fluorocarbon-functionalized nanoparticles	IR780	pH-sensitive fluorocarbon/ iRGD	PDT	149
Lipid-polymer/PFC	Ce6	Perfluoro-octan-1-ol affinity O ₂	PDT	150
Upconversion nanoparticles with RBC	Rose bengal	RBC deliver O ₂	PDT	151
RBC/ammonium bicarbonate/DOX	ICG	RBC deliver O ₂	Chem/ PTT /PDT	152
Amphiphilic triblock copolymers	ZnPc	Hemoglobin deliver O ₂	PDT	153
Hemoglobin conjugated polymer nanoparticles	Luminol	Hemoglobin deliver O ₂	PDT	154
Catalase-loaded hierarchical zeolite	Methylene blue	Catalase generate O ₂	PDT	155
HSA-Ce6-catalase-PTX nanoparticles	Ce6	Catalase generate O ₂	Chemo-PDT	157
PTX/ICG-nanovehicles@Au@ catalase nanoparticles	ICG	Catalase generate O ₂	PDT/PTT	159
UCNPs @ZIF-8@catalase	Methylene blue	Catalase generate O ₂	PDT	160
Catalase@S/Ce6-CTPP/DPEG	Ce6	Catalase generate O ₂	Immuno-PDT	161
Catalase-entrapped nanocapsules	Porphyrin	Catalase generate O ₂	PDT	162
Catalase-integrated hyaluronic acid	Ce6	Catalase generate O ₂	PDT	163
Black phosphorus/MnO ₂	Black phosphorus	MnO ₂ generate O ₂	PDT	164
Magnetofluorescent Carbon Dot	Phthalocyanine	MnO ₂ nanodots generate O ₂	PDT	167
Mn-Cdots/DOX-loaded mesoporous silica-coated gold cube nanocomposites	Phthalocyanine	MnO ₂ nanodots generate O ₂	PDT/PTT	168
PLGA/hematoporphyrin monomethyl ether @MnO ₂	Porphyrin	MnO ₂ generate O ₂	PDT	169
Upconversion composite nanoparticles	Ce6	MnO ₂ generate O ₂	PDT	170
Ce6@MnO ₂ -PEG nanoparticles	Ce6	MnO ₂ generate O ₂	PDT	167
Hydrangea MnO ₂ /DOX	aza-BODIPY	MnO ₂ generate O ₂	PDT	175
Semiconducting hybrid nanoparticles	PCPDTBT	MnO ₂ generate O ₂	PDT	176
MnFe ₂ O ₄ -anchored mesoporous silica	Ce6	Fenton reaction	PDT	178
MnFe ₂ O ₄ @Metal-organic frameworks	Porphyrin	Fenton reaction/ consume GSH	PDT	179
MoS ₂ /rGO-MnO ₂ -PEG	Reduced graphene oxide	p-n heterojunction/ MnO ₂ generate O ₂	PDT	180
F127-MnO ₂ -ZIF@DOX/C ₃ N ₄	C ₃ N ₄	MnO ₂ nanodots generate O ₂	Chemo-PDT	181
Pt Metal-organic frameworks	Porphyrin	Pt nanozymes produce O ₂	PDT	185
Pd@Pt-PEG-Ce6	Ce6	Pt nanozymes produce O ₂	PDT/PTT	186
H ₂ O ₂ /PLGA	IR780	H ₂ O ₂ release O ₂	PDT	187
UCNP@mSiO ₂ @ZIF-90-DOX-PEGFA	Rose bengal	ZIF-90 reserve O ₂	Chemo-PDT	188
UCNP with hyperbaric oxygen	Rose bengal	Hyperbaric oxygen supply O ₂	PDT	189
Carbon dots/TiO ₂ nanotubes	Carbon dots	Carbon dots enhance light absorption	PDT	195
TiO ₂ -ruthenium nano-photosensitizer	Organometallic ruthenium	N ₃ injected electrons into TiO ₂	PDT	196
Carbon-dot-doped C ₃ N ₄ / amphipathic polymer	PpIX	C ₃ N ₄ split water to generate O ₂	PDT	199
Fe ^{III} -doped-C ₃ N ₄ nanofusiform	Methylene blue	H ₂ O ₂ -activatable, O ₂ -evolving, mitochondrial-target	PDT	200
Cu ^{II} -doped-C ₃ N ₄	C ₃ N ₄	Reduce GSH	PDT	201
Ulathrin Graphdiyne oxide/iRGD peptide-modified RBC	Graphdiyne oxide	sufficient O ₂ / tumor cell targeting /penetrating	PDT/PTT	202

Table 3. Physical effects of nanoplatforms for enhanced PDT

Nanoplatforms design	PS	Enhanced mechanism	Improved therapeutics	Ref
Ion-incorporated silicate nanoscintillators	Rose bengal	X-rays transmit the energy to PS	PDT	213
Mesoporous LaF ₃ :Tb nanoparticles	Rose bengal	X-rays transmit the energy to PS	PDT	216
LiLuF ₄ :Ce@SiO ₂ @Ag ₃ PO ₄ @Pt(IV)	LiLuF ₄ :Ce	X-rays transmit the energy to PS	PDT	218
CeF ₃ :Gd ³⁺ ,Tb ³⁺ @SiO ₂	Rose bengal	X-rays transmit the energy to PS	PDT/ radiotherapy	219
Gold nanorods@ SiO ₂	(Eu) complexes	X-rays transmit the energy to PS	PDT/PTT	220
PLGA /Gold nanoparticles	Verteporfin	X-rays transmit the energy to PS	PDT	222
Silica-gold nanorod	ICG	SPR	PDT	225
UCNP-gold nanorod	Methylene blue	SPR	PDT	226
Gold nanoparticles with black phosphorus	Black phosphorus	SPR	PDT/PTT	227
Multilayered upconversion	PFSBT	Resonance energy transfer	PDT	232
SnWO ₄ -based nano hybrids	SnWO ₄	Resonance energy transfer	PDT/ radiotherapy	233
Dyad molecule with pluronic F-127-folic acid	BODIPY	Resonance energy transfer	PDT	234

**Figure 14.** Illustration showing the preparation process and mechanisms underlying the effects of X-PDT with LiLuF₄:Ce@SiO₂@Ag₃PO₄@Pt(IV) nanoparticles (LAPNP). Adapted with permission from ref. [218]. Copyright 2018 American Chemical Society.

Other nanoplatforms through resonance energy transfer

Although conventional single chromophore-based PS like porphyrin derivatives [228], methyl blue [229], rose bengal [230], merocyanine 540 [231], and heavy metal complexes possess therapeutic capabilities for cancer, their absorption intensities and ¹O₂ generation efficiencies in the NIR region are not

ideal. To improve NIR-mediated PDT of the existing PS, UCNPs have been developed as *in vivo* phototransducers that could emit in the visible spectrum when excited by NIR light, overlapping with the activation wavelengths of the existing PS. Liu *et al.* constructed a multilayered upconversion nanoplatform consisting of three functional layers, where the upconversion nanoparticles served as the core and light-sensitive conjugated polymers and apo-

transferrin-titanocene (Tf@Tc) as shells [232]. Under NIR irradiation, apparent energy transfer occurred from the core to the polymer and Tc components in the shell, producing ROS and free radicals for cancer cell killing. *In vitro* cellular assays revealed the synergistic therapeutic effect of the conjugated polymer and Tc as PS. *In vivo* studies showed that tumor growth was significantly inhibited in mice receiving the theranostic platform and NIR irradiation. Also, the tin tungstate (SnWO_4) generated great attention, because its unique band structure has remarkable visible light active photocatalytic performance, which is not found in any other tungsten-based binary or ternary compounds. Zhang *et al.* developed hybrid nanoplatforms based on the conjugation of needle-like SnWO_4 nanocrystals and UCNP [233]. The UCNP-emitted light of the nanoplatform was effectively absorbed by SnWO_4 , triggering the type-I PDT process to activate ROS maxima. The strong X-ray attenuation capacity of both tungsten and tin elements qualified the USWs as excellent radio-sensitizers for radiotherapy enhancement, which played a complementary role in PDT treatment. The quantum efficiency of UCNP and consequent PDT outcomes are still suboptimal

and relatively high-power intensity of the laser excitation sources are typically required. To extend NIR PS options with improved $^1\text{O}_2$ efficiency, NIR-absorbing dyad PS based on resonance energy transfer have been developed, which have increased absorption intensity to maximize the use of absorbed photons, and greatly improve the efficiency in concomitant $^1\text{O}_2$ generation. Huang *et al.* developed a dyad molecule based on the integration of the energy-donor moiety (distyryl-BODIPY) and PS (diiodo-distyryl-BODIPY) by click chemistry [234]. The dyad molecules encapsulated with biodegradable copolymer pluronic F127-folic acid could form uniform and water-soluble nanoparticles (Figure 15A), and displayed significantly enhanced absorption and $^1\text{O}_2$ efficiency relative to that of the acceptor moiety of the PS alone in the NIR region. *In vitro* RET-BDP-TNM showed higher fluorescence intensity than RETBDP-NNM because of the folic acid ligand at the tumor site (Figure 15B). With an exceptionally low-power NIR LED light irradiation, tumor growth (group 6) was significantly suppressed, as shown in Figure 15C and 15D. This result indicated RET-BDP-TNM could produce strong tumor PDT.

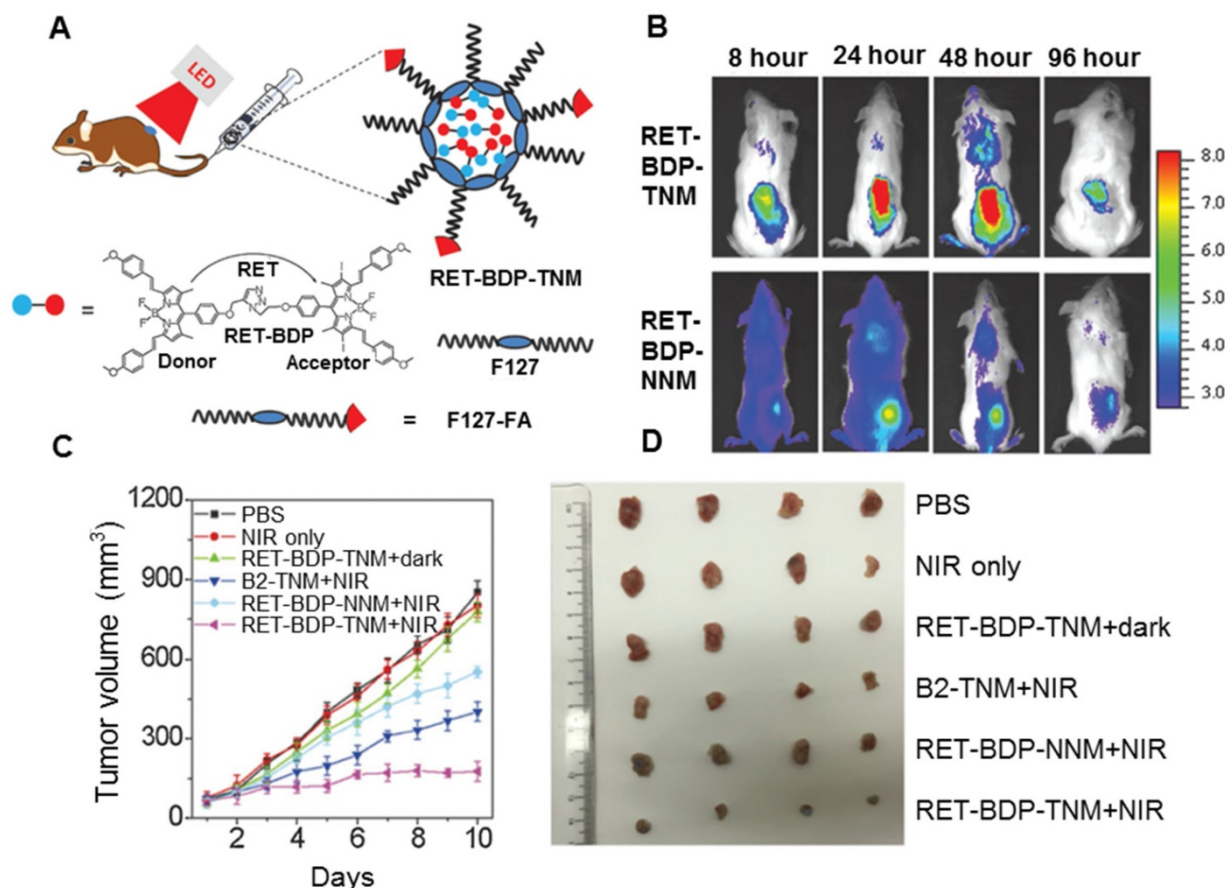


Figure 15. NIR photosensitized nanoparticles for enhanced PDT. **A.** Schematic illustration of RET-photosensitizer-mediated PDT. **B.** Specific targeted NIR-fluorescence tumor imaging *in vivo*. **C.** Tumor growth inhibition by RET-BDP-TNM-mediated PDT in 4T1 tumors. **D.** Digital photos of tumors for the four groups of mice. Adapted with permission from ref. [234]. Copyright 2017 Wiley-VCH.

Conclusions and Perspective

Overall, noninvasive PDT represents an effective and highly selective tumor-ablative therapy in clinical applications. Good therapeutic effect and the possibility of the parallel application of PDT with other therapeutic protocols make it a frequently used strategy in many fields of medicine. In this review, we summarized the latest achievements and breakthroughs in constructing versatile nanoplatfoms for enhanced PDT from a broad perspective. A variety of effective and proven approaches, such as stimulating a responsive release, tumor-targeting ability, O₂ self-sufficient property, photocatalytic performance, physical effect (X-rays and surface plasmon resonance), and improvement through resonance energy transfer, were also discussed in detail.

Despite remarkable progress, there are still several considerable challenges facing the preparation of engineered nanoplatfoms and their translation into clinical practice. Traditional nanoplatfoms usually experience early recognition by the immune system and quick clearance from blood circulation, leading to low accumulation at the tumor site. Although some targeting nanoplatfoms enhanced PDT, the local concentration was still relatively low compared to the total administered dose. Since the average distance of ¹O₂ diffusion is around 100 nm, targeting groups on nanoplatfoms can increase their internalization in tumor cells for enhanced PDT. Thus, in the future, multiple organelle-targeting functions need to be explored for PDT, involving molecular recognition of overexpressed cellular receptors in the targeted area. Besides imparting tumor selectivity, another critical area to focus on is preventing unwanted side effects of nanoplatfoms to the living organisms, thereby ensuring their compatibility and biosafety.

Currently, the performance of PS has limitations. Therefore, exploration of new PS, especially with high efficiency, is a primary focus in photodynamic research. The current complicated methods may have an impact on the application and performance of nanoplatfoms. Therefore, another area of pursuit is of the relatively simple and smart methods for engineering nanoplatfoms with sophisticated synthetic processes and formulations. However, another major challenge is the fundamental clinical requirements for the mass production of these nanoplatfoms. For example, biodegraded hollow MOF-based nanoplatfoms possess an efficacious PS loading capacity and maintain the high oxygen yield. Additionally, physicochemical characterization of nanoplatfoms in terms of size, zeta potential, surface

chemistry, colloidal stability, and, most importantly, safety protocols are needed.

The biggest payoff of versatile nanoplatfoms contributes to the realization of theranostics, the integrated function of therapy and diagnostics by a single nanoformulation. For example, real-time monitoring of the therapeutic action is desired *in vitro* and even *in vivo*. It would be highly significant to provide real-time and on-site outcomes for patients for their post-treatment evaluation. Besides, it has been reported that PDT might result in cancer resistance at the cellular and molecular level. Combining PDT with different therapeutic modalities, such as chemotherapy or photothermal therapy, is crucial for further optimization of therapeutic efficiency. The mechanisms underlying the synergy between multi-modal theranostics need to be explored. In particular, the therapeutic effect of 1+1 = >2 must be exerted rather than the additive effect of the individual features, the mechanism of synergy between multi-modal theranostics also needs to be deeply explored. The combination of different modalities is expected to provide functional compensation, diagnostic accuracy, and improved therapeutic efficiency.

Finally, most of the tumors are located deep inside the body rather than on the surface, requiring improved deep penetrating ability of PDT for deep-seated therapy. Immunotherapy has recently gained immense credence for eliminating distant metastatic cancer cells and remove residual cancer cells in the body. Thus, the synergistic use of deep tissue PDT and immunotherapy offers unique advantages in treating both deep-seated primary tumors and distant metastatic tumors. The successful translation of these nanoplatfoms to clinical applications is anticipated in the near future upon satisfactory tackling of the current critical issues.

Acknowledgements

This work was supported by the National Natural Science Foundation of China (51803112, 216740859), China Postdoctoral Science Foundation Grant (2018M633503), Key Laboratory Construction Program of Xi'an Municipal Bureau of Science and Technology (201805056ZD7CG40), and Innovation Capability Support Program of Shaanxi (No. 2018PT-28, 2019PT-05).

Competing Interests

The authors have declared that no competing interest exists.

References

- Ostrand GK, Cheng KC, Wolf JC, Wolfe MJ. Shark cartilage, cancer and the growing threat of pseudoscience. *Cancer Res.* 2004; 64: 8485-91.
- Shi J, Kantoff PW, Wooster R, Farokhzad OC. Cancer nanomedicine: progress, challenges and opportunities. *Nat Rev Cancer.* 2017; 17: 20.
- Wolfgang CL, Herman JM, Laheru DA, Klein AP, Erdek MA, Fishman EK, et al. Recent progress in pancreatic cancer. *CA Cancer J Clin.* 2013; 63: 318-48.
- Vahrmeijer AL, Hutteman M, Van Der Vorst JR, Van De Velde CJ, Frangioni JV. Image-guided cancer surgery using near-infrared fluorescence. *Nat Rev Clin Oncol.* 2013; 10: 507.
- Zhong Y, Meng F, Deng C, Zhong Z. Ligand-directed active tumor-targeting polymeric nanoparticles for cancer chemotherapy. *Biomacromolecules.* 2014; 15: 1955-169.
- Her S, Jaffray DA, Allen C. Gold nanoparticles for applications in cancer radiotherapy: Mechanisms and recent advancements. *Adv Drug Deliv Rev.* 2017; 109: 84-101.
- Bartelink H, Maingon P, Poortmans P, Weltens C, Fourquet A, Jager J, et al. Whole-breast irradiation with or without a boost for patients treated with breast-conserving surgery for early breast cancer: 20-year follow-up of a randomised phase 3 trial. *Lancet Oncol.* 2015; 16: 47-56.
- Wu Q, Yang Z, Nie Y, Shi Y, Fan D. Multi-drug resistance in cancer chemotherapeutics: mechanisms and lab approaches. *Cancer Lett.* 2014; 347: 159-66.
- Zhang XD, Luo Z, Chen J, Shen X, Song S, Sun Y, et al. Ultrasmall Au10-12(SG)10-12 nanomolecules for high tumor specificity and cancer radiotherapy. *Adv Mater.* 2014; 26: 4565-8.
- Roelandts R. The history of phototherapy: something new under the sun? *J Am Acad Dermatol.* 2002; 46: 926-30.
- Xie Z, Chen S, Duo Y, Zhu Y, Fan T, Zou Q, et al. Biocompatible two-dimensional titanium nanosheets for multimodal imaging-guided cancer theranostics. *ACS Appl Mater Interfaces.* 2019; 11: 22129-40.
- Xie Z, Duo Y, Lin Z, Fan T, Xing C, Yu L, et al. The rise of 2D photothermal materials beyond graphene for clean water production. *Adv Sci.* 2020; 7: 1902236.
- Xing C, Chen S, Qiu M, Liang X, Liu Q, Zou Q, et al. Black phosphorus hydrogels: conceptually novel black phosphorus/cellulose hydrogels as promising photothermal agents for effective cancer therapy. *Adv Healthc Mater.* 2018; 7: 1870030.
- Zhu X, Feng W, Chang J, Tan Y-W, Li J, Chen M, et al. Temperature-feedback upconversion nanocomposite for accurate photothermal therapy at facile temperature. *Nat Commun.* 2016; 7: 10437.
- Chen Q, Xu L, Liang C, Wang C, Peng R, Liu Z. Photothermal therapy with immune-adjutant nanoparticles together with checkpoint blockade for effective cancer immunotherapy. *Nat Commun.* 2016; 7: 1-13.
- Zou L, Wang H, He B, Zeng L, Tan T, Cao H, et al. Current approaches of photothermal therapy in treating cancer metastasis with nanotherapeutics. *Theranostics.* 2016; 6: 762.
- Lucky SS, Soo KC, Zhang Y. Nanoparticles in photodynamic therapy. *Chem Rev.* 2015; 115: 1990-2042.
- Fan W, Huang P, Chen X. Overcoming the Achilles' heel of photodynamic therapy. *Chem Soc Rev.* 2016; 45: 6488-519.
- Vohra F, Al-Kheraif AA, Qadri T, Hassan MIA, Ahmed A, Warnakulasuriya S, et al. Efficacy of photodynamic therapy in the management of oral premalignant lesions. A systematic review. *Photodiagnosis Photodyn Ther.* 2015; 12: 150-9.
- Lucena SR, Salazar N, Gracia-Cazaña T, Zamarrón A, González S, Juaranz A, et al. Combined treatments with photodynamic therapy for non-melanoma skin cancer. *Int J Mol Sci.* 2015; 16: 25912-33.
- Lu K, He C, Lin W. Nanoscale metal-organic framework for highly effective photodynamic therapy of resistant head and neck cancer. *J Am Chem Soc.* 2014; 136: 16712-5.
- He C, Liu D, Lin W. Self-assembled core-shell nanoparticles for combined chemotherapy and photodynamic therapy of resistant head and neck cancers. *ACS Nano.* 2015; 9: 991-1003.
- Wang D, Fei B, Halig LV, Qin X, Hu Z, Xu H, et al. Targeted iron-oxide nanoparticle for photodynamic therapy and imaging of head and neck cancer. *ACS Nano.* 2014; 8: 6620-32.
- Bhowmick R, Girotti AW. Pro-survival and pro-growth effects of stress-induced nitric oxide in a prostate cancer photodynamic therapy model. *Cancer Lett.* 2014; 343: 115-22.
- Perera M, Krishnananthan N, Lindner U, Lawrentschuk N. An update on focal therapy for prostate cancer. *Nat Rev Urol.* 2016; 13: 641.
- Shafirstein G, Battoo A, Harris K, Baumann H, Gollnick SO, Lindenmann J, et al. Photodynamic therapy of non-small cell lung cancer. narrative review and future directions. *Ann Am Thorac Soc.* 2016; 13: 265-75.
- Yue C, Yang Y, Zhang C, Alfranca G, Cheng S, Ma L, et al. ROS-responsive mitochondria-targeting blended nanoparticles: chemo-and photodynamic synergistic therapy for lung cancer with on-demand drug release upon irradiation with a single light source. *Theranostics.* 2016; 6: 2352.
- Wang H, Yu D, Fang J, Cao C, Liu Z, Ren J, et al. Renal-clearable porphyrinic metal-organic framework nanodots for enhanced photodynamic therapy. *ACS Nano.* 2019; 13: 9206-17.
- Liu Z, Liu X, Du Y, Ren J, Qu X. Using plasmonic copper sulfide nanocrystals as smart light-driven sterilants. *ACS Nano.* 2015; 9: 10335-46.
- Lovell JF, Liu TW, Chen J, Zheng G. Activatable photosensitizers for imaging and therapy. *Chem Rev.* 2010; 110: 2839-57.
- Jung HS, Han J, Shi H, Koo S, Singh H, Kim H-J, et al. Overcoming the limits of hypoxia in photodynamic therapy: a carbonic anhydrase IX-targeted approach. *J Am Chem Soc.* 2017; 139: 7595-602.
- Zhou Z, Song J, Nie L, Chen X. Reactive oxygen species generating systems meeting challenges of photodynamic cancer therapy. *Chem Soc Rev.* 2016; 45: 6597-626.
- Liu Y, Liu Y, Bu W, Cheng C, Zuo C, Xiao Q, et al. Hypoxia induced by upconversion-based photodynamic therapy: towards highly effective synergistic bioreductive therapy in tumors. *Angew Chem Int Ed.* 2015; 54: 8105-9.
- Feng L, Cheng L, Dong Z, Tao D, Barnhart TE, Cai W, et al. Theranostic liposomes with hypoxia-activated prodrug to effectively destruct hypoxic tumors post-photodynamic therapy. *ACS Nano.* 2016; 11: 927-37.
- Mallidi S, Watanabe K, Timmerman D, Schoenfeld D, Hasan T. Prediction of tumor recurrence and therapy monitoring using ultrasound-guided photoacoustic imaging. *Theranostics.* 2015; 5: 289.
- Fargnoli MC, Peris K. Photodynamic therapy for basal cell carcinoma. *Future Oncol.* 2015; 11: 2991-6.
- Song G, Cheng L, Chao Y, Yang K, Liu Z. Emerging nanotechnology and advanced materials for cancer radiation therapy. *Adv Mater.* 2017; 29: 1700996.
- Homayoni H, Rashidi LH, Chen W. Combination of photodynamic therapy and nanotechnology: non-invasive weapon against cancer. *Rev Nanosci Nanotechnol.* 2014; 3: 107-32.
- Obaid G, Broekgaarden M, Bulin A-L, Huang H-C, Kuriakose J, Liu J, et al. Photonanomedicine: a convergence of photodynamic therapy and nanotechnology. *Nanoscale.* 2016; 8: 12471-503.
- Tsujimoto H, Morimoto Y, Takahata R, Nomura S, Yoshida K, Horiguchi H, et al. Photodynamic therapy using nanoparticle loaded with indocyanine green for experimental peritoneal dissemination of gastric cancer. *Cancer Sci.* 2014; 105: 1626-30.
- Bhaumik J, Mittal AK, Banerjee A, Chisti Y, Banerjee UC. Applications of phototheranostic nanoagents in photodynamic therapy. *Nano Res.* 2015; 8: 1373-94.
- Sun Q, He F, Bi H, Wang Z, Sun C, Li C, et al. An intelligent nanoplatform for simultaneously controlled chemo-, photothermal, and photodynamic therapies mediated by a single NIR light. *Chem Eng J.* 2019; 362: 679-91.
- Zhao R, Liang X, Zhao B, Chen M, Liu R, Sun S, et al. Ultrasound assisted gene and photodynamic synergistic therapy with multifunctional FOXA1-siRNA loaded porphyrin microbubbles for enhancing therapeutic efficacy for breast cancer. *Biomaterials.* 2018; 173: 58-70.
- Chen J, Fan T, Xie Z, Zeng Q, Xue P, Zheng T, et al. Advances in nanomaterials for photodynamic therapy applications: Status and challenges. *Biomaterials.* 2020; 237: 119827.
- Clauson RM, Chen M, Scheetz LM, Berg B, Chertok B. Size-controlled iron oxide nanoplatforms with lipidoid-stabilized shells for efficient magnetic resonance imaging-trackable lymph node targeting and high-capacity biomolecule display. *ACS Appl Mater Interfaces.* 2018; 10: 20281-95.
- Wang J, Zhao H, Zhou Z, Zhou P, Yan Y, Wang M, et al. MR/SPECT imaging guided photothermal therapy of tumor-targeting Fe@Fe₃O₄ nanoparticles in vivo with low mononuclear phagocyte uptake. *ACS Appl Mater Interfaces.* 2016; 8: 19872-82.
- Xue F, Wei P, Ge X, Zhong Y, Cao C, Yu D, et al. A pH-responsive organic photosensitizer specifically activated by cancer lysosomes. *Dyes Pigm.* 2018; 156: 285-90.
- Choi YS, Kwon K, Yoon K, Huh KM, Kang HC. Photosensitizer-mediated mitochondria-targeting nanosized drug carriers: subcellular targeting, therapeutic, and imaging potentials. *Int J Pharm.* 2017; 520: 195-206.
- de Bruijn HS, Mashayekhi V, Schreurs TJJ, van Driel PBAA, Strijkers GJ, van Diest PJ, et al. Acute cellular and vascular responses to photodynamic therapy using EGFR-targeted nanobody-photosensitizer conjugates studied with intravital optical imaging and magnetic resonance imaging. *Theranostics.* 2020; 10: 2436-52.
- Luk BT, Zhang L. Cell membrane-camouflaged nanoparticles for drug delivery. *J Control Release.* 2015; 220: 600-7.
- Yang Y, Yu J, Monemian Esfahani A, Seiffert-Sinha K, Xi N, Lee I, et al. Single-cell membrane drug delivery using porous pen nanodeposition. *Nanoscale.* 2018; 10: 12704-12.
- Feng Y, Chen W, Jia Y, Tian Y, Zhao Y, Long F, et al. N-Heterocyclic molecule-capped gold nanoparticles as effective antibiotics against multi-drug resistant bacteria. *Nanoscale.* 2016; 8: 13223-7.
- Liu L-H, Qiu W-X, Zhang Y-H, Li B, Zhang C, Gao F, et al. A charge reversible self-delivery chimeric peptide with cell membrane-targeting properties for enhanced photodynamic therapy. *Adv Funct Mater.* 2017; 27: 1700220.
- Luo G-F, Chen W-H, Hong S, Cheng Q, Qiu W-X, Zhang X-Z. A self-transformable pH-driven membrane-anchoring photosensitizer for effective photodynamic therapy to inhibit tumor growth and metastasis. *Adv Funct Mater.* 2017; 27: 1702122.
- Zhong J, Li L, Zhu X, Guan S, Yang Q, Zhou Z, et al. A smart polymeric platform for multistage nucleus-targeted anticancer drug delivery. *Biomaterials.* 2015; 65: 43-55.
- Pan L, Liu J, Shi J. Intracellular photosensitizer delivery and photosensitization for enhanced photodynamic therapy with ultralow irradiance. *Adv Funct Mater.* 2014; 24: 7318-27.

57. Yang Y, Zhu W, Feng L, Chao Y, Yi X, Dong Z, et al. G-quadruplex-based nanoscale coordination polymers to modulate tumor hypoxia and achieve nuclear-targeted drug delivery for enhanced photodynamic therapy. *Nano Lett.* 2018; 18: 6867-75.
58. Shadel GS, Horvath TL. Mitochondrial ROS signaling in organismal homeostasis. *Cell.* 2015; 163: 560-9.
59. Chouchani ET, Kazak L, Jedrychowski MP, Lu GZ, Erickson BK, Szpyt J, et al. Mitochondrial ROS regulate thermogenic energy expenditure and sulfenylation of UCP1. *Nature.* 2016; 532: 112-6.
60. Morgan J, Oseroff AR. Mitochondria-based photodynamic anti-cancer therapy. *Adv Drug Deliv Rev.* 2001; 49: 71-86.
61. Hilf R. Mitochondria are targets of photodynamic therapy. *J Bioenerg Biomembr.* 2007; 39: 85-9.
62. Tong H, Du J, Li H, Jin Q, Wang Y, Ji J. Programmed photosensitizer conjugated supramolecular nanocarriers with dual targeting ability for enhanced photodynamic therapy. *Chem Commun.* 2016; 52: 11935-8.
63. Cheng H, Zheng R-R, Fan G-L, Fan J-H, Zhao L-P, Jiang X-Y, et al. Mitochondria and plasma membrane dual-targeted chimeric peptide for single-agent synergistic photodynamic therapy. *Biomaterials.* 2019; 188: 1-11.
64. Li B, Ge Gb, Wen L, Yuan Y, Zhang R, Peng X, et al. A lysosomal probe for monitoring of pH in living cells and ovarian tumour. *Dyes Pigm.* 2017; 139: 318-25.
65. Tsubone TM, Martins WK, Pavani C, Junqueira HC, Itri R, Baptista MS. Enhanced efficiency of cell death by lysosome-specific photodamage. *Sci Rep.* 2017; 7: 6734.
66. Xiang H-J, Deng Q, An L, Guo M, Yang S-P, Liu J-G. Tumor cell specific and lysosome-targeted delivery of nitric oxide for enhanced photodynamic therapy triggered by 808 nm near-infrared light. *Chem Commun.* 2016; 52: 148-51.
67. Lv W, Zhang Z, Zhang KY, Yang H, Liu S, Xu A, et al. A mitochondria-targeted photosensitizer showing improved photodynamic therapy effects under hypoxia. *Angew Chem Int Ed.* 2016; 55: 9947-51.
68. Okabe Y, Medzhitov R. Tissue biology perspective on macrophages. *Nat Immunol.* 2015; 17: 9.
69. Wan D-H, Zheng B-Y, Ke M-R, Duan J-Y, Zheng Y-Q, Yeh C-K, et al. C-Phycocyanin as a tumour-associated macrophage-targeted photosensitizer and a vehicle of phthalocyanine for enhanced photodynamic therapy. *Chem Commun.* 2017; 53: 4112-5.
70. Adimoolam MG, A V, Nalam MR, Sunkara MV. Chlorin e6 loaded lactoferrin nanoparticles for enhanced photodynamic therapy. *J Mater Chem B.* 2017; 5: 9189-96.
71. Kong SD, Zhang W, Lee JH, Brammer K, Lal R, Karin M, et al. Magnetically vectored nanocapsules for tumor penetration and remotely switchable on-demand drug release. *Nano Lett.* 2010; 10: 5088-92.
72. Yang G, Sun X, Liu J, Feng L, Liu Z. Light-Responsive, Singlet-oxygen-triggered on-demand drug release from photosensitizer-doped mesoporous silica nanorods for cancer combination therapy. *Adv Funct Mater.* 2016; 26: 4722-32.
73. Kai Y, Min C, Zhou S, Wu L. Self-assembly of upconversion nanoclusters with an amphiphilic copolymer for near-infrared- and temperature-triggered drug release. *RSC Adv.* 2016; 6: 85293-302.
74. Kankala RK, Kuthati Y, Liu C-L, Lee C-H. Hierarchical coated metal hydroxide nanoconstructs as potential controlled release carriers of photosensitizer for skin melanoma. *RSC Adv.* 2015; 5: 42666-80.
75. Yu M, Guo F, Wang J, Tan F, Li N. Photosensitizer-loaded pH-responsive hollow gold nanospheres for single light-induced photothermal/photodynamic therapy. *ACS Appl Mater Interfaces.* 2015; 7: 17592-7.
76. Turan IS, Yildiz D, Turksoy A, Gunaydin G, Akkaya EU. A bifunctional photosensitizer for enhanced fractional photodynamic therapy: singlet oxygen generation in the presence and absence of light. *Angew Chem Int Ed.* 2016; 55: 2875-8.
77. Di Corato R, Béalle G, Kolosnjaj-Tabi J, Espinosa A, Clement O, Silva AK, et al. Combining magnetic hyperthermia and photodynamic therapy for tumor ablation with photoresponsive magnetic liposomes. *ACS Nano.* 2015; 9: 2904-16.
78. Yao J, Feng J, Chen J. External-stimuli responsive systems for cancer theranostic. *Asian J Pharm Sci.* 2016; 11: 585-95.
79. Yan K, Yu J, Zhang B, Wu L. Novel fluorinated polymer-mediated upconversion nanoclusters for pH/redox triggered anticancer drug release and intracellular imaging. *Macromol Chem Phys.* 2017; 218: 170090.
80. Claassen C, Gerlach T, Rother D. Stimulus-responsive regulation of enzyme activity for one-step and multi-step syntheses. *Adv Synth Catal.* 2019; 361: 2387-401.
81. Li R, Peng F, Cai J, Yang D, Zhang P. Redox dual-stimuli responsive drug delivery systems for improving tumor-targeting ability and reducing adverse side effects. *Asian J Pharm Sci.* 2019; DOI: 10.1016/j.ajps.201906003.
82. Zhang W, Wang F, Wang Y, Wang J, Yu Y, Guo S, et al. pH and near-infrared light dual-stimuli responsive drug delivery using DNA-conjugated gold nanorods for effective treatment of multidrug resistant cancer cells. *J Control Release.* 2016; 232: 9-19.
83. Karimi M, Eslami M, Sahandi-Zangabad P, Mirab F, Farajisafiloo N, Shafaei Z, et al. pH-sensitive stimulus-responsive nanocarriers for targeted delivery of therapeutic agents. *Wiley Interdiscip Rev Nanomed Nanobiotechnol.* 2016; 8: 696-716.
84. Faggi E, Serra-Vinardell J, Pandey MD, Casas J, Fabriàs G, Luis SV, et al. Pseudopeptidic fluorescent on-off pH sensor based on pyrene excimer emission: imaging of acidic cellular organelles. *Sens Actuators B Chem.* 2016; 234: 633-40.
85. Ma X, Gong N, Zhong L, Sun J, Liang X-J. Future of nanotherapeutics: targeting the cellular sub-organelles. *Biomaterials.* 2016; 97: 10-21.
86. Penfold NJW, Lovett JR, Warren NJ, Verstraete P, Smets J, Armes SP. pH-responsive non-ionic diblock copolymers: protonation of a morpholine end-group induces an order-order transition. *Polym Chem.* 2016; 7: 79-88.
87. Zhang C, An T, Wang D, Wan G, Zhang M, Wang H, et al. Stepwise pH-responsive nanoparticles containing charge-reversible pullulan-based shells and poly(β -amino ester)/poly(lactic-co-glycolic acid) cores as carriers of anticancer drugs for combination therapy on hepatocellular carcinoma. *J Control Release.* 2016; 226: 193-204.
88. Tong H, Wang Y, Li H, Jin Q, Ji J. Dual pH-responsive 5-aminolevulinic acid pseudopolyrotaxane prodrug micelles for enhanced photodynamic therapy. *Chem Commun.* 2016; 52: 3966-9.
89. Chu W-Y, Tsai M-H, Peng C-L, Shih Y-H, Luo T-Y, Yang S-J, et al. pH-responsive nanophotosensitizer for an enhanced photodynamic therapy of colorectal cancer overexpressing EGFR. *Mol Pharm.* 2018; 15: 1432-44.
90. Han S-S, Li Z-Y, Zhu J-Y, Han K, Zeng Z-Y, Hong W, et al. Dual-pH sensitive charge-reversal polypeptide micelles for tumor-triggered targeting uptake and nuclear drug delivery. *Small.* 2015; 11: 2543-54.
91. Jing Y, Xiong X, Ming Y, Zhao J, Guo X, Yang G, et al. A multifunctional micellar nanoplatfrom with pH-triggered cell penetration and nuclear targeting for effective cancer therapy and inhibition to lung metastasis. *Adv Healthc Mater.* 2018; 7: 1700974.
92. Li F, Du Y, Liu J, Sun H, Wang J, Li R, et al. Responsive assembly of upconversion nanoparticles for pH-activated and near-infrared-triggered photodynamic therapy of deep tumors. *Adv Mater.* 2018; 30: 1802808.
93. Huang Z, Huang L, Huang Y, He Y, Sun X, Fu X, et al. Phthalocyanine-based coordination polymer nanoparticles for enhanced photodynamic therapy. *Nanoscale.* 2017; 9: 15883-94.
94. Kong F, Liang Z, Luan D, Liu X, Xu K, Tang B. A glutathione (GSH)-responsive near-infrared (NIR) theranostic prodrug for cancer therapy and imaging. *Anal Chem.* 2016; 88: 6450-6.
95. Li M, Wu X, Wang Y, Li Y, Zhu W, James TD. A near-infrared colorimetric fluorescent chemodosimeter for the detection of glutathione in living cells. *Chem Commun.* 2014; 50: 1751-3.
96. Idelchik MdPS, Begley U, Begley TJ, Melendez JA. Mitochondrial ROS control of cancer. *Semin Cancer Biol.* 2017; 47: 57-66.
97. Deng Y, Jia F, Chen S, Shen Z, Jin Q, Fu G, et al. Nitric oxide as an all-rounder for enhanced photodynamic therapy: hypoxia relief, glutathione depletion and reactive nitrogen species generation. *Biomaterials.* 2018; 187: 55-65.
98. Feng L, He F, Dai Y, Gai S, Zhong C, Li C, et al. Multifunctional UCNP@MnSiO₃@g-C₃N₄ nanoplatfrom: improved ROS generation and reduced glutathione levels for highly efficient photodynamic therapy. *Biomater Sci.* 2017; 5: 2456-67.
99. Elkassih SA, Kos P, Xiong H, Siegwart DJ. Degradable redox-responsive disulfide-based nanogel drug carriers via dithiol oxidation polymerization. *Biomater Sci.* 2019; 7: 607-17.
100. Zhou Y, Jie K, Huang F. A dual redox-responsive supramolecular amphiphile fabricated by selenium-containing pillar[6]arene-based molecular recognition. *Chem Commun.* 2018; 54: 12856-9.
101. Chen Y, Rui L, Liu L, Zhang W. Redox-responsive supramolecular amphiphiles based on a pillar[5]arene for enhanced photodynamic therapy. *Polym Chem.* 2016; 7: 3268-76.
102. Xue Y, Tian J, Liu Z, Chen J, Wu M, Shen Y, et al. A redox stimulation-activated amphiphile for enhanced photodynamic therapy. *Biomacromolecules.* 2019; 20: 2796-808.
103. Lin S, Lei K, Du W, Yang L, Shi H, Gao Y, et al. Enhancement of oxaliplatin sensitivity in human colorectal cancer by hypericin mediated photodynamic therapy via ROS-related mechanism. *Int J Biochem Cell Biol.* 2016; 71: 24-34.
104. Guan Q, Li Y-A, Li W-Y, Dong Y-B. Photodynamic therapy based on nanoscale metal-organic frameworks: from material design to cancer nanotherapeutics. *Chem Asian J.* 2018; 13: 3122-49.
105. Zhang W, Lu J, Gao X, Li P, Zhang W, Ma Y, et al. Enhanced photodynamic therapy by reduced levels of intracellular glutathione obtained by employing a nano-MOF with Cu^{II} as the active center. *Angew Chem Int Ed.* 2018; 57: 4891-6.
106. Zeng Q, Zhang R, Zhang T, Xing D. H₂O₂-responsive biodegradable nanomedicine for cancer-selective dual-modal imaging guided precise photodynamic therapy. *Biomaterials.* 2019; 207: 39-48.
107. Wang Q, Sun M, Li D, Li C, Luo C, Wang Z, et al. Cytochrome P450 enzyme-mediated auto-enhanced photodynamic cancer therapy of co-nanoassembly between clopidogrel and photosensitizer. *Theranostics.* 2020; 10: 5550-64.
108. Gong H, Chao Y, Xiang J, Han X, Song G, Feng L, et al. Hyaluronidase to enhance nanoparticle-based photodynamic tumor therapy. *Nano Lett.* 2016; 16: 2512-21.
109. Li W, Zheng C, Pan Z, Chen C, Hu D, Gao G, et al. Smart hyaluronidase-activated theranostic micelles for dual-modal imaging guided photodynamic therapy. *Biomaterials.* 2016; 101: 10-9.
110. Ross D, Kepa JK, Winski SL, Beall HD, Anwar A, Siegel D. NAD(P)H:quinone oxidoreductase 1 (NQO1): chemoprotection, bioactivation, gene regulation and genetic polymorphisms. *Chem Biol Interact.* 2000; 129: 77-97.

111. Yao C, Li Y, Wang Z, Song C, Hu X, Liu S. Cytosolic NQO1 enzyme-activated near-infrared fluorescence imaging and photodynamic therapy with polymeric vesicles. *ACS Nano*. 2020; 14: 1919-35.
112. Wu Q, Ni X. ROS-mediated DNA methylation pattern alterations in carcinogenesis. *Curr Drug Targets*. 2015; 16: 13-9.
113. Zhang Y, Liao H, Zhong S, Gao F, Chen Y, Huang Z, et al. Effect of N-n-butyl haloperidol iodide on ROS/JNK/Egr-1 signaling in H9c2 cells after hypoxia/reoxygenation. *Sci Rep*. 2015; 5: 11809.
114. Lin Y, Lin H, Lin Y, Zhang S, Chen Y, Jiang X. The roles of metabolism of membrane lipids and phenolics in hydrogen peroxide-induced pericarp browning of harvested longan fruit. *Postharvest Biol Technol*. 2016; 111: 53-61.
115. Zhao J, Ma J, Deng Y, Kelly JA, Kim K, Bang S-Y, et al. A missense variant in NCF1 is associated with susceptibility to multiple autoimmune diseases. *Nat Genet*. 2017; 49: 433.
116. Ritchie RH, Drummond GR, Sobey CG, De Silva TM, Kemp-Harper BK. The opposing roles of NO and oxidative stress in cardiovascular disease. *Pharmacol Res*. 2017; 116: 57-69.
117. Saravanakumar G, Lee J, Kim J, Kim WJ. Visible light-induced singlet oxygen-mediated intracellular disassembly of polymeric micelles co-loaded with a photosensitizer and an anticancer drug for enhanced photodynamic therapy. *Chem Commun*. 2015; 51: 9995-8.
118. Li J, Meng X, Deng J, Lu D, Zhang X, Chen Y, et al. Multifunctional micelles dually responsive to hypoxia and singlet oxygen: enhanced photodynamic therapy via interactively triggered photosensitizer delivery. *ACS Appl Mater Interfaces*. 2018; 10: 17117-28.
119. Hu L, Gao S, Ding X, Wang D, Jiang J, Jin J, et al. Photothermal-responsive single-walled carbon nanotube-based ultrathin membranes for on/off switchable separation of oil-in-water nanoemulsions. *ACS Nano*. 2015; 9: 4835-42.
120. Wang Y, Li S, Zhang P, Bai H, Feng L, Lv F, et al. Photothermal-responsive conjugated polymer nanoparticles for remote control of gene expression in living cells. *Adv Mater*. 2018; 30: 1705418.
121. Xu X, Chong Y, Liu X, Fu H, Yu C, Huang J, et al. Multifunctional nanotheranostic gold nanocages for photoacoustic imaging guided radio/photodynamic/photothermal synergistic therapy. *Acta Biomater*. 2019; 84: 328-38.
122. Yin D, Li X, Ma Y, Liu Z. Targeted cancer imaging and photothermal therapy via monosaccharide-imprinted gold nanorods. *Chem Commun*. 2017; 53: 6716-9.
123. Lv Q, Gao M-Y, Cheng Z-H, Chen Q, Shen A-G, Hu J-M. Rational synthesis of hollow cubic CuS@Spiky Au core-shell nanoparticles for enhanced photothermal and SERS effects. *Chem Commun*. 2018; 54: 13399-402.
124. Geng B, Qin H, Shen W, Li P, Fang F, Li X, et al. Carbon dot/Ws₂ heterojunctions for NIR-II enhanced photothermal therapy of osteosarcoma and bone regeneration. *Chem Eng J*. 2019; 383: 123102.
125. Liu B, Li C, Chen G, Liu B, Deng X, Wei Y, et al. Synthesis and optimization of MoS₂@Fe₃O₄-ICG/Pt(IV) nanoflowers for MR/IR/PA bioimaging and combined PTT/PDT/chemotherapy triggered by 808 nm laser. *Adv Sci*. 2017; 4: 1600540.
126. Wang D, Ren Y, Shao Y, Yu D, Meng L. Facile preparation of doxorubicin-loaded and folic acid-conjugated carbon nanotubes@Poly(N-vinyl pyrrole) for targeted synergistic chemo-photothermal cancer treatment. *Bioconjug Chem*. 2017; 28: 2815-22.
127. Gulzar A, Xu J, Yang D, Xu L, He F, Gai S, et al. Nano-graphene oxide-UCNP-Ce6 covalently constructed nanocomposites for NIR-mediated bioimaging and PTT/PDT combinatorial therapy. *Dalton Trans*. 2018; 47: 3931-9.
128. Meng Y, Wang S, Li C, Qian M, Yan X, Yao S, et al. Photothermal combined gene therapy achieved by polyethyleneimine-grafted oxidized mesoporous carbon nanospheres. *Biomaterials*. 2016; 100: 134-42.
129. Ocsoy I, Isiklan N, Cansiz S, Özdemir N, Tan W. ICG-conjugated magnetic graphene oxide for dual photothermal and photodynamic therapy. *RSC Adv*. 2016; 6: 30285-92.
130. Wang K, Zhang Y, Wang J, Yuan A, Sun M, Wu J, et al. Self-assembled IR780-loaded transferrin nanoparticles as an imaging, targeting and PDT/PTT agent for cancer therapy. *Sci Rep*. 2016; 6: 1-11.
131. Bharathiraja S, Manivasagan P, Santha Moorthy M, Bui NQ, Jang B, Phan TTV, et al. Photo-based PDT/PTT dual model killing and imaging of cancer cells using phycocyanin-polypyrrole nanoparticles. *Eur J Pharm Biopharm*. 2018; 123: 20-30.
132. Cao S, Tong X, Dai K, Xu Q. A super-stretchable and tough functionalized boron nitride/PEDOT:PSS/poly(N-isopropylacrylamide) hydrogel with self-healing, adhesion, conductive and photothermal activity. *J Mater Chem A*. 2019; 7: 8204-9.
133. Jiang W, Mo F, Jin X, Chen L, Xu LJ, Guo L, et al. Tumor-targeting photothermal heating-responsive nanoplateform based on reduced graphene oxide/mesoporous silica/hyaluronic acid nanocomposite for enhanced photodynamic therapy. *Adv Mater Interfaces*. 2017; 4: 1700425.
134. El Bakkari M, McClenaghan N, Vincent J-M. The pyridyl-tag strategy applied to the hydrocarbon/perfluorocarbon phase-switching of a porphyrin and a fullerene. *J Am Chem Soc*. 2002; 124: 12942-3.
135. Xu Y, Xu J, Hu X, Xia X, Dong Q, Liu Z, et al. Zinc-substituted hemoglobin with specific drug binding sites and fatty acid resistance ability for enhanced photodynamic therapy. *Nano Res*. 2019; 12: 1880-7.
136. Li G, Yuan S, Deng D, Ou T, Li Y, Sun R, et al. Fluorinated polyethylenimine to enable transmucosal delivery of photosensitizer-conjugated catalase for photodynamic therapy of orthotopic bladder tumors postintravesical instillation. *Adv Funct Mater*. 2019; 29: 1901932.
137. Liu P, Ren J, Xiong Y, Yang Z, Zhu W, He Q, et al. Enhancing magnetic resonance/photoluminescence imaging-guided photodynamic therapy by multiple pathways. *Biomaterials*. 2019; 199: 52-62.
138. Yang Z, Wang J, Ai S, Sun J, Mai X, Guan W. Self-generating oxygen enhanced mitochondrion-targeted photodynamic therapy for tumor treatment with hypoxia scavenging. *Theranostics*. 2019; 9: 6809-23.
139. Kirsch P. *Modern fluoroorganic chemistry: synthesis, reactivity, applications*. John Wiley & Sons. 2013.
140. Yao Y, Liu X, Liu T, Zhou J, Zhu J, Sun G, et al. Preparation of inclusion complex of perfluorocarbon compound with β -cyclodextrin for ultrasound contrast agent. *RSC Adv*. 2015; 5: 6305-10.
141. Tirotta I, Dichiarante V, Pigliacelli C, Cavallo G, Terraneo G, Bombelli FB, et al. ¹⁹F magnetic resonance imaging (MRI): from design of materials to clinical applications. *Chem Rev*. 2015; 115: 1106-29.
142. Yao Y, Zhang M, Liu T, Zhou J, Gao Y, Wen Z, et al. Perfluorocarbon-encapsulated PLGA-PEG emulsions as enhancement agents for highly efficient reoxygenation to cell and organism. *ACS Appl Mater Interfaces*. 2015; 7: 18369-78.
143. Khalighi Z, Rahmani A, Cheraghi J, Ahmadi MRH, Soleimannejad K, Asadollahi R, et al. Perfluorocarbon attenuates inflammatory cytokines, oxidative stress and histopathologic changes in paraquat-induced acute lung injury in rats. *Environ Toxicol Pharmacol*. 2016; 42: 9-15.
144. Scheer A, Kirsch M, Ferenz KB. Perfluorocarbons in photodynamic and photothermal therapy. *J Nanosci Nanomed*. 2017; 1: 21-7.
145. Ren H, Liu J, Li Y, Wang H, Ge S, Yuan A, et al. Oxygen self-enriched nanoparticles functionalized with erythrocyte membranes for long circulation and enhanced phototherapy. *Acta Biomater*. 2017; 59: 269-82.
146. Ren H, Liu J, Su F, Ge S, Yuan A, Dai W, et al. Relighting photosensitizers by synergistic integration of albumin and perfluorocarbon for enhanced photodynamic therapy. *ACS Appl Mater Interfaces*. 2017; 9: 3463-73.
147. Yu M, Xu X, Cai Y, Zou L, Shuai X. Perfluorohexane-cored nanodroplets for stimulations-responsive ultrasonography and O₂-potentiated photodynamic therapy. *Biomaterials*. 2018; 175: 61-71.
148. Tao D, Feng L, Chao Y, Liang C, Song X, Wang H, et al. Covalent organic polymers based on fluorinated porphyrin as oxygen nanoshuttles for tumor hypoxia relief and enhanced photodynamic therapy. *Adv Funct Mater*. 2018; 28: 1804901.
149. Ma S, Zhou J, Zhang Y, Yang B, He Y, Tian C, et al. An oxygen self-sufficient fluorinated nanoplateform for relieved tumor hypoxia and enhanced photodynamic therapy of cancers. *ACS Appl Mater Interfaces*. 2019; 11: 7731-42.
150. Song R, Hu D, Chung HY, Sheng Z, Yao S. Lipid-polymer bilaminar oxygen nanobubbles for enhanced photodynamic therapy of cancer. *ACS Appl Mater Interfaces*. 2018; 10: 36805-13.
151. Wang P, Li X, Yao C, Wang W, Zhao M, El-Toni AM, et al. Orthogonal near-infrared upconversion co-regulated site-specific O₂ delivery and photodynamic therapy for hypoxia tumor by using red blood cell microcarriers. *Biomaterials*. 2017; 125: 90-100.
152. Wan G, Chen B, Li L, Wang D, Shi S, Zhang T, et al. Nanoscaled red blood cells facilitate breast cancer treatment by combining photothermal/photodynamic therapy and chemotherapy. *Biomaterials*. 2018; 155: 25-40.
153. Wang S, Yuan F, Chen K, Chen G, Tu K, Wang H, et al. Synthesis of hemoglobin conjugated polymeric micelle: a ZnPc carrier with oxygen self-compensating ability for photodynamic therapy. *Biomacromolecules*. 2015; 16: 2693-700.
154. Jiang L, Bai H, Liu L, Lv F, Ren X, Wang S. Luminescent, Oxygen-supplying, hemoglobin-linked conjugated polymer nanoparticles for photodynamic therapy. *Angew Chem*. 2019; 131: 10770-5.
155. Hu D, Chen Z, Sheng Z, Gao D, Yan F, Ma T, et al. A catalase-loaded hierarchical zeolite as an implantable nanocapsule for ultrasound-guided oxygen self-sufficient photodynamic therapy against pancreatic cancer. *Nanoscale*. 2018; 10: 17283-92.
156. Zhao J, Fei J, Du C, Cui W, Ma H, Li J. Assembly of catalase-based bioconjugates for enhanced anticancer efficiency of photodynamic therapy in vitro. *Chem Commun*. 2013; 49: 10733-5.
157. Chen Q, Chen J, Liang C, Feng L, Dong Z, Song X, et al. Drug-induced co-assembly of albumin/catalase as smart nano-theranostics for deep intra-tumoral penetration, hypoxia relieve, and synergistic combination therapy. *J Control Release*. 2017; 263: 79-89.
158. Zhang L, Yang XQ, Wei JS, Li X, Wang H, Zhao YD. Intelligent gold nanostars for in vivo CT imaging and catalase-enhanced synergistic photodynamic & photothermal tumor therapy. *Theranostics*. 2019; 9: 5424-42.
159. He Y, Cong C, He Y, Hao Z, Li C, Wang S, et al. Tumor hypoxia relief overcomes multidrug resistance and immune inhibition for self-enhanced photodynamic therapy. *Chem Eng J*. 2019; 375: 122079.
160. Cai H-J, Shen T-T, Zhang J, Shan C-F, Jia J-G, Li X, et al. A core-shell metal-organic-framework (MOF)-based smart nanocomposite for efficient NIR/H₂O₂-responsive photodynamic therapy against hypoxic tumor cells. *J Mater Chem B*. 2017; 5: 2390-4.

161. Yang G, Xu L, Xu J, Zhang R, Song G, Chao Y, et al. Smart nanoreactors for pH-responsive tumor homing, mitochondria-targeting, and enhanced photodynamic-immunotherapy of cancer. *Nano Lett.* 2018; 18: 2475-84.
162. Wang H, Chao Y, Liu J, Zhu W, Wang G, Xu L, et al. Photosensitizer-crosslinked in-situ polymerization on catalase for tumor hypoxia modulation & enhanced photodynamic therapy. *Biomaterials.* 2018; 181: 310-7.
163. Phua SZE, Yang G, Lim WQ, Verma A, Chen H, Thanabalu T, et al. Catalase-integrated hyaluronic acid as nanocarriers for enhanced photodynamic therapy in solid tumor. *ACS Nano.* 2019; 13: 4742-51.
164. Chen Y, Ye D, Wu M, Chen H, Zhang L, Shi J, et al. Break-up of two-dimensional MnO₂ nanosheets promotes ultrasensitive pH-triggered theranostics of cancer. *Adv Mater.* 2014; 26: 7019-26.
165. Gordijo CR, Abbasi AZ, Amini MA, Lip HY, Maeda A, Cai P, et al. Design of hybrid MnO₂-polymer-lipid nanoparticles with tunable oxygen generation rates and tumor accumulation for cancer treatment. *Adv Funct Mater.* 2015; 25: 1858-72.
166. Liu J, Du P, Liu T, Wong BJC, Wang W, Ju H, et al. A black phosphorus/manganese dioxide nanoplateform: oxygen self-supply monitoring, photodynamic therapy enhancement and feedback. *Biomaterials.* 2019; 192: 179-88.
167. Jia Q, Ge J, Liu W, Zheng X, Chen S, Wen Y, et al. A magnetofluorescent carbon dot assembly as an acidic H₂O₂-driven oxygenator to regulate tumor hypoxia for simultaneous bimodal imaging and enhanced photodynamic therapy. *Adv Mater.* 2018; 30: 1706090.
168. Zhang X, Xi Z, Machuki JOa, Luo J, Yang D, Li J, et al. Gold cube-in-cube based oxygen nanogenerator: a theranostic nanoplateform for modulating tumor microenvironment for precise chemo-phototherapy and multimodal imaging. *ACS Nano.* 2019; 13: 5306-25.
169. Hao Y, Zhang B, Zheng C, Niu M, Guo H, Zhang H, et al. Multifunctional nanoplateform for enhanced photodynamic cancer therapy and magnetic resonance imaging. *Colloids Surf B Biointerfaces.* 2017; 151: 384-93.
170. Gu T, Cheng L, Gong F, Xu J, Li X, Han G, et al. Upconversion composite nanoparticles for tumor hypoxia modulation and enhanced near-infrared-triggered photodynamic therapy. *ACS Appl Mater Interfaces.* 2018; 10: 15494-503.
171. Wu K, Zhao H, Sun Z, Wang B, Tang X, Dai Y, et al. Endogenous oxygen generating multifunctional theranostic nanoplateform for enhanced photodynamic-photothermal therapy and multimodal imaging. *Theranostics.* 2019; 9: 7697-713.
172. Zhu W, Dong Z, Fu T, Liu J, Chen Q, Li Y, et al. Modulation of hypoxia in solid tumor microenvironment with MnO₂ nanoparticles to enhance photodynamic therapy. *Adv Funct Mater.* 2016; 26: 5490-8.
173. Balsukuri N, Lone MY, Jha PC, Mori S, Gupta I. Synthesis, structure, and optical studies of donor-acceptor-type near-infrared (NIR) aza-boron-dipyrromethene (BODIPY) dyes. *Chem Asian J.* 2016; 11: 1572-87.
174. Gawale Y, Adarsh N, Kalva SK, Joseph J, Pramanik M, Ramaiah D, et al. Carbazole-linked near-infrared Aza-BODIPY dyes as triplet sensitizers and photoacoustic contrast agents for deep-tissue imaging. *Chem Eur J.* 2017; 23: 6570-8.
175. Tang Q, Cheng Z, Yang N, Li Q, Wang P, Chen D, et al. Hydrangea-structured tumor microenvironment responsive degradable nanoplateform for hypoxic tumor multimodal imaging and therapy. *Biomaterials.* 2019; 205: 1-10.
176. Zhu H, Li J, Qi X, Chen P, Pu K. Oxygenic hybrid semiconducting nanoparticles for enhanced photodynamic therapy. *Nano Lett.* 2018; 18: 586-94.
177. Bi H, Dai Y, Yang P, Xu J, Yang D, Gai S, et al. Glutathione and H₂O₂ consumption promoted photodynamic and chemotherapy based on biodegradable MnO₂-Pt@Au₂₅ nanosheets. *Chem Eng J.* 2019; 356: 543-53.
178. Kim J, Cho HR, Jeon H, Kim D, Song C, Lee N, et al. Continuous O₂-evolving MnFe₂O₄ nanoparticle-anchored mesoporous silica nanoparticles for efficient photodynamic therapy in hypoxic cancer. *J Am Chem Soc.* 2017; 139: 10992-5.
179. Yin S-Y, Song G, Yang Y, Zhao Y, Wang P, Zhu L-M, et al. Persistent regulation of tumor microenvironment via circulating catalysis of MnFe₂O₄@metal-organic frameworks for enhanced photodynamic therapy. *Adv Funct Mater.* 2019; 29: 1901417.
180. Kapri S, Bhattacharyya S. Molybdenum sulfide-reduced graphene oxide p-n heterojunction nanosheets with anchored oxygen generating manganese dioxide nanoparticles for enhanced photodynamic therapy. *Chem Sci.* 2018; 9: 8982-9.
181. Zhang W, Li S, Liu X, Yang C, Hu N, Dou L, et al. Oxygen-generating MnO₂ nanodots-anchored versatile nanoplateform for combined chemo-photodynamic therapy in hypoxic cancer. *Adv Funct Mater.* 2018; 28: 1706375.
182. Lin Y, Ren J, Qu X. Catalytically active nanomaterials: a promising candidate for artificial enzymes. *Acc Chem Res.* 2014; 47: 1097-105.
183. Wu J, Wang X, Wang Q, Lou Z, Li S, Zhu Y, et al. Nanomaterials with enzyme-like characteristics (nanozymes): next-generation artificial enzymes (II). *Chem Soc Rev.* 2019; 48: 1004-76.
184. Liu Y, Wu H, Li M, Yin JJ, Nie Z. pH dependent catalytic activities of platinum nanoparticles with respect to the decomposition of hydrogen peroxide and scavenging of superoxide and singlet oxygen. *Nanoscale.* 2014; 6: 11904-10.
185. Zhang Y, Wang F, Liu C, Wang Z, Kang L, Huang Y, et al. Nanozyme decorated metal-organic frameworks for enhanced photodynamic therapy. *ACS Nano.* 2018; 12: 651-61.
186. Wei J, Li J, Sun D, Li Q, Ma J, Chen X, et al. A novel theranostic nanoplateform based on Pd@Pt-PEG-Ce6 for enhanced photodynamic therapy by modulating tumor hypoxia microenvironment. *Adv Funct Mater.* 2018; 28: 1706310.
187. Wang B, Lin W, Mao Z, Gao C. Near-infrared light triggered photothermal therapy and enhanced photodynamic therapy with a tumor-targeting hydrogen peroxide shuttle. *J Mater Chem B.* 2018; 6: 3145-55.
188. Xie Z, Cai X, Sun C, Liang S, Shao S, Huang S, et al. O₂-loaded pH-responsive multifunctional nanodrug carrier for overcoming hypoxia and highly efficient chemo-photodynamic cancer therapy. *Chem Mater.* 2019; 31: 483-90.
189. Li J, Huang J, Ao Y, Li S, Miao Y, Yu Z, et al. Synergizing upconversion nanophotosensitizers with hyperbaric oxygen to remodel the extracellular matrix for enhanced photodynamic cancer therapy. *ACS Appl Mater Interfaces.* 2018; 10: 22985-96.
190. Hisatomi T, Kubota J, Domen K. Recent advances in semiconductors for photocatalytic and photoelectrochemical water splitting. *Chem Soc Rev.* 2014; 43: 7520-35.
191. Wang W, Xu X, Zhou W, Shao Z. Recent progress in metal-organic frameworks for applications in electrocatalytic and photocatalytic water splitting. *Adv Sci.* 2017; 4: 1600371.
192. Cui H, Zhao W, Yang C, Yin H, Lin T, Shan Y, et al. Black TiO₂ nanotube arrays for high-efficiency photoelectrochemical water-splitting. *J Mater Chem A.* 2014; 2: 8612-6.
193. Ge M, Li Q, Cao C, Huang J, Li S, Zhang S, et al. One-dimensional TiO₂ nanotube photocatalysts for solar water splitting. *Adv Sci.* 2017; 4: 1600152.
194. Wang W, Dong J, Ye X, Li Y, Ma Y, Qi L. Heterostructured TiO₂ nanorod@nanobowl arrays for efficient photoelectrochemical water splitting. *Small.* 2016; 12: 1469-78.
195. Yang D, Yang G, Sun Q, Gai S, He F, Dai Y, et al. Carbon-dot-decorated TiO₂ nanotubes toward photodynamic therapy based on water-splitting mechanism. *Adv Healthc Mater.* 2018; 7: 1800042.
196. Gilson RC, Black KCL, Lane DD, Achilefu S. Hybrid TiO₂-ruthenium nano-photosensitizer synergistically produces reactive oxygen species in both hypoxic and normoxic conditions. *Angew Chem Int Ed.* 2017; 56: 10717-20.
197. Zheng D, Cao X-N, Wang X. Precise formation of a hollow carbon nitride structure with a janus surface to promote water splitting by photoredox catalysis. *Angew Chem Int Ed.* 2016; 55: 11512-6.
198. Zhang K, Wang L, Sheng X, Ma M, Jung MS, Kim W, et al. Tunable bandgap energy and promotion of H₂O₂ oxidation for overall water splitting from carbon nitride nanowire bundles. *Adv Energy Mater.* 2016; 6: 1502352.
199. Zheng D-W, Li B, Li C-X, Fan J-X, Lei Q, Li C, et al. Carbon-dot-decorated carbon nitride nanoparticles for enhanced photodynamic therapy against hypoxic tumor via water splitting. *ACS Nano.* 2016; 10: 8715-22.
200. Ma Z, Zhang M, Jia X, Bai J, Ruan Y, Wang C, et al. Fe^{III}-doped two-dimensional C₃N₄ nanofusiform: a new O₂-evolving and mitochondria-targeting photodynamic agent for MRI and enhanced antitumor therapy. *Small.* 2016; 12: 5477-87.
201. Ju E, Dong K, Chen Z, Liu Z, Liu C, Huang Y, et al. Copper^{II}-graphitic carbon nitride triggered synergy: improved ROS generation and reduced glutathione levels for enhanced photodynamic therapy. *Angew Chem.* 2016; 128: 11639-43.
202. Jiang W, Zhang Z, Wang Q, Dou J, Zhao Y, Ma Y, et al. Tumor reoxygenation and blood perfusion enhanced photodynamic therapy using ultrathin graphdiyne oxide nanosheets. *Nano Lett.* 2019; 19: 4060-7.
203. Mang TS. Lasers and light sources for PDT: past, present and future. *Photodiagnosis Photodyn Ther.* 2004; 1: 43-8.
204. Dalong N, Ferreira C, Jiang D, Chen W, Cao T, Sun T, et al. Cerenkov radiation-induced photodynamic therapy amplified by magnetic nanotheranostics. *J Nucl Med.* 2019; 60: 661-661.
205. Kulbacka J. Nanosecond pulsed electric fields (nsPEFs) impact and enhanced photofrin II@ delivery in photodynamic reaction in cancer and normal cells. *Photodiagnosis Photodyn Ther.* 2015; 12: 621-9.
206. Chu X, Li K, Guo H, Zheng H, Shuda S, Wang X, et al. Exploration of graphitic-C₃N₄ quantum dots for microwave-induced photodynamic therapy. *ACS Biomater Sci Eng.* 2017; 3: 1836-44.
207. Wu Q, Xia N, Long D, Tan L, Rao W, Yu J, et al. Dual-functional supernanoparticles with microwave dynamic therapy and microwave thermal therapy. *Nano Lett.* 2019; 19: 5277-86.
208. Chu X, Mao L, Johnson O, Li K, Phan J, Yin Q, et al. Exploration of TiO₂ nanoparticle mediated microdynamic therapy on cancer treatment. *Nanomedicine.* 2019; 18: 272-81.
209. Zheng X, Liu W, Ge J, Jia Q, Nan F, Ding Y, et al. Biodegradable natural product-based nanoparticles for near-infrared fluorescence imaging-guided sonodynamic therapy. *ACS Appl Mater Interfaces.* 2019; 11: 18178-85.
210. Yan H, Shang W, Sun X, Zhao L, Wang J, Xiong Z, et al. "All-in-One" nanoparticles for trimodality imaging-guided intracellular photo-magnetic hyperthermia therapy under intravenous administration. *Adv Funct Mater.* 2018; 28: 1705710.
211. Li M, Zhao J, Chu H, Mi Y, Zhou Z, Di Z, et al. Light-activated nanoprobe for biosensing and imaging. *Adv Mater.* 2019; 31: 1804745.
212. Ren X-D, Hao X-Y, Li H-C, Ke M-R, Zheng B-Y, Huang J-D. Progress in the development of nanosensitizers for X-ray-induced photodynamic therapy. *Drug Discov Today.* 2018; 23: 1791-800.

213. Sun W, Shi T, Luo L, Chen X, Lv P, Lv Y, et al. Monodisperse and uniform mesoporous silicate nanosensitizers achieve low-dose X-ray-induced deep-penetrating photodynamic therapy. *Adv Mater.* 2019; 31: 1808024.
214. Chen X, Song J, Chen X, Yang H. X-ray-activated nanosystems for theranostic applications. *Chem Soc Rev.* 2019; 48: 3073-101.
215. Sun W, Zhou Z, Pratz G, Chen X, Chen H. Nanoscintillator-mediated X-ray induced photodynamic therapy for deep-seated tumors: from concept to biomedical applications. *Theranostics.* 2020; 10: 1296.
216. Liu Y, Chen W, Wang S, Joly AG. Investigation of water-soluble x-ray luminescence nanoparticles for photodynamic activation. *Appl Phys Lett.* 2008; 92: 043901.
217. Tang Ya, Hu J, Elmenoufy AH, Yang X. Highly efficient FRET system capable of deep photodynamic therapy established on X-ray excited mesoporous LaF₃:Tb scintillating nanoparticles. *ACS Appl Mater Interfaces.* 2015; 7: 12261-9.
218. Wang H, Lv B, Tang Z, Zhang M, Ge W, Liu Y, et al. Scintillator-based nanohybrids with sacrificial electron prodrug for enhanced X-ray-Induced photodynamic therapy. *Nano Lett.* 2018; 18: 5768-74.
219. Ahmad F, Wang X, Jiang Z, Yu X, Liu X, Mao R, et al. Codoping enhanced radioluminescence of nanoscintillators for X-ray-activated synergistic cancer therapy and prognosis using metabolomics. *ACS Nano.* 2019; 13: 10419-33.
220. Luo L, Sun W, Feng Y, Qin R, Zhang J, Ding D, et al. Conjugation of a scintillator complex and gold nanorods for dual-modal image-guided photothermal and X-ray-induced photodynamic therapy of tumors. *ACS Appl Mater Interfaces.* 2020; 12: 12591-9.
221. Ren X, Hao X, Li H, Ke M, Zheng B, Huang J. Progress in the development of nanosensitizers for X-ray-induced photodynamic therapy. *Drug Discov Today.* 2018; 23: 1791-800.
222. Deng W, McKelvey KJ, Guller A, Fayzullin A, Campbell JM, Clement S, et al. Application of mitochondrially targeted nanoconstructs to neoadjuvant X-ray-induced photodynamic therapy for rectal cancer. *ACS Central Sci.* 2020. DOI: org/10.1021/acscentsci.9b01121.
223. Hong F, Tang C, Xue Q, Zhao L, Shi H, Hu B, et al. Simultaneously enhanced singlet oxygen and fluorescence production of nanoplatform by surface plasmon resonance coupling for biomedical applications. *Langmuir.* 2019; 35 :14833-14839.
224. Li B, Tan L, Liu X, Li Z, Cui Z, Liang Y, et al. Superimposed surface plasma resonance effect enhanced the near-infrared photocatalytic activity of Au@Bi₂WO₆ coating for rapid bacterial killing. *J Hazard Mater.* 2019; 380: 120818.
225. Li Y, Wen T, Zhao R, Liu X, Ji T, Wang H, et al. Localized electric field of plasmonic nanoplatform enhanced photodynamic tumor therapy. *ACS Nano.* 2014; 8: 11529-42.
226. Chen C-W, Chan Y-C, Hsiao M, Liu R-S. Plasmon-enhanced photodynamic cancer therapy by up conversion nanoparticles conjugated with Au nanorods. *ACS Appl Mater Interfaces.* 2016; 8: 32108-19.
227. Zhang D, Lin X, Lan S, Sun H, Wang X, Liu X, et al. Localized surface plasmon resonance enhanced singlet oxygen generation and light absorption based on black phosphorus@AuNPs nanosheet for tumor photodynamic/thermal therapy. *Part Part Syst Charact.* 2018; 35: 1800010.
228. Kou J, Dou D, Yang L. Porphyrin photosensitizers in photodynamic therapy and its applications. *Oncotarget.* 2017; 8: 81591.
229. Maciel CM, Piva MR, Ribeiro MAG, de Santana Santos T, Ribeiro CF, Martins-filho PRS. Methylene blue-mediated photodynamic inactivation followed by low-laser therapy versus miconazole gel in the treatment of denture stomatitis. *J Prosthodont.* 2016; 25: 28-32.
230. Wang B, Wang J-H, Liu Q, Huang H, Chen M, Li K, et al. Rose-bengal-conjugated gold nanorods for in vivo photodynamic and photothermal oral cancer therapies. *Biomaterials.* 2014; 35: 1954-66.
231. Wang S, Yang W, Cui J, Li X, Dou Y, Su L, et al. pH- and NIR light responsive nanocarriers for combination treatment of chemotherapy and photodynamic therapy. *Biomater Sci.* 2016; 4: 338-45.
232. Liu S, Yuan Y, Yang Y, Liu Z, Yin S, Qin W, et al. Multilayered upconversion nanocomposites with dual photosensitizing functions for enhanced photodynamic therapy. *J Mater Chem B.* 2017; 5: 8169-77.
233. Zhang M, Cui Z, Song R, Lv B, Tang Z, Meng X, et al. SnWO₄-based nanohybrids with full energy transfer for largely enhanced photodynamic therapy and radiotherapy. *Biomaterials.* 2018; 155: 135-44.
234. Huang L, Li Z, Zhao Y, Yang J, Yang Y, Pendharkar AI, et al. Enhancing photodynamic therapy through resonance energy transfer constructed near-infrared photosensitized nanoparticles. *Adv Mater.* 2017; 29: 1604789.